CHAPTER 4

Ship Seakeeping

Chapter Outline

4.1. Introduction

Seakeeping of ships is investigated with respect to the following issues:

- Maximum speed in a seaway: 'involuntary' speed reduction due to added resistance in waves and 'voluntary' speed reduction to avoid excessive motions, loads, etc.
- Route optimization (routing) to minimize, e.g., transport time, fuel consumption, or total cost.
- Structural design of the ship with respect to loads in seaways.
- Habitation comfort and safety of people on board: motion sickness, danger of accidental falls, man overboard.

Practical Ship Hydrodynamics. DOI: 10.1016/B978-0-08-097150-6.10004-1

- Ship safety: capsizing, large roll motions and accelerations, slamming, wave impact on superstructures or deck cargo, propeller racing resulting in excessive rpm for the engine.
- Operational limits for ships (e.g. for offshore supply vessels or helicopters landing on ships).

Tools to predict ship seakeeping are:

- Model tests.
- Full-scale measurements on ships at sea.
- Computations in the frequency domain: determination of the ship reactions to harmonic waves of different wave lengths and wave directions.
- Computations in the time domain (simulation in time): computation of the forces on the ship for given motions at one point in time; based on that information the computation of the motions at a following point in time, etc.
- Computations in the statistical domain: computation of statistically significant seakeeping values in natural (irregular) seaways, e.g. average frequency (occurrence per time) of events, such as exceeding certain limits for motions or loads in a given seaway or ocean region.

For many seakeeping issues, seakeeping is determined as follows:

1. Representation of the natural seaway as superposition of many regular (harmonic) waves (Fourier decomposition).
2. Computation (or sometimes measurement in model tests) of the ship reactions of interest in these harmonic waves.
3. Addition of the reactions in all these harmonic waves to a total reaction (superposition).

This procedure assumes (respectively requires) that the reaction of one wave on the ship is not changed by the simultaneous occurrence of another wave. This assumption is valid for small wave heights for almost all ship reactions with the exception of the added resistance.

This procedure is often applied also for seaways with large waves. However, in these cases it can only give rough estimates requiring proper corrections. One consequence of the assumed independence of the individual wave reactions is that all reactions of the ship are proportional to wave height. This is called linearization with respect to wave height.

The computations become considerably more expensive if this simplification is not made. Non-linear computations are usually necessary for the treatment of extreme motions (e.g. for capsizing investigations); here simulation in the time domain is the proper tool. However, for the determination of maximum loads it often suffices to apply corrections to initially linearly computed loads. The time-averaged added resistance is in good approximation proportional to the square of the wave height. Here the effect of harmonic waves of different lengths and direction can be superimposed as for the linear ship reactions.

To determine global properties (e.g. ship motions and accelerations) with sufficient accuracy, simpler methods suffice than for the determination of local properties (pressures, relative motions between water and ship).

Further recommended reading includes Faltinsen (1993, 2005) and Lewis (1990).

4.2. Experimental Approaches (Model and Full Scale)

Seakeeping model tests usually employ self-propelled models in narrow towing tanks or broad, rectangular seakeeping basins. The models are sometimes completely free, being kept on course by a rudder operated in remote control or by an autopilot. In other cases, some degrees of freedom are suppressed (e.g. by wires). If internal forces and moments are to be determined, the model is divided into a number of sections. The individual watertight sections are coupled to each other by gauges. These gauges consist of two rigid frames connected by rather stiff flat springs with strain gauges. Model motions are determined either directly or by measuring the accelerations and integrating them twice in time. Waves and relative motions of ships and waves are measured using two parallel wires penetrating the water surface. The change in the voltage between the wires is then correlated to the depth of submergence in water. The accuracy of ultrasonic devices is slightly worse. The model position in the tank can be determined from the angles between the ship and two or more cameras at the tank side. Either lights or reflectors on the ship give the necessary clear signal.

The waves are usually created by flaps driven by hydraulic cylinders. The flaps are inclined around a horizontal axis lying at the height of the tank bottom or even lower. Traditionally, these flaps were controlled mechanically by shaft mechanisms which created a (nearly) sinusoidal motion. Modern wave-makers are computer controlled following a prescribed time function. Sinusoidal flap motion creates harmonic waves. The superposition of many sinusoidal waves of different frequency creates irregular waves similar to natural wind seas. Some wave-makers use heightwise segmented flaps to simulate better the exponential decay of waves with water depth. Sometimes, but much less frequently, vertically moved bodies or air cushions are used to generate waves. These facilities create not only the desired wave, but also a near-field disturbance which decays with distance from the body or the air cushion. More harmful is the generation of higher harmonics (waves with an integer multiple of the basic wave frequency), but these higher harmonics can be easily filtered from the measured reactions if the reactions are linear. In computer-controlled wave-makers they can be largely eliminated by proper adjustment of the flap motions.

In towing tanks, waves are usually generated by one flap at one tank end spanning the complete tank width. The other tank end has a ‘beach’ to absorb the waves (ideally completely) so that no reflected waves influence the measurements and the water comes to rest as soon as possible after a test. If several, independently controlled flaps are used over the tank width, waves with

propagation direction oblique to the tank longitudinal axis can be generated. These waves will then be reflected at the side walls of the tank. This is unproblematic if a superposition of many waves of different direction ('short-crested sea') is created as long as the distribution of the wave energy over the propagation direction is symmetrical to the tank longitudinal axis. In natural wind seas the energy distribution is similarly distributed around the average wind direction.

Rectangular wide seakeeping basins typically have a large number of wave-making flaps at two adjacent sides. An appropriate phase shift in the flap motions can then create oblique wave propagation. The other two sides of such a basin are then equipped with 'beaches' to absorb waves.

Seakeeping model tests are usually only performed for strongly non-linear seakeeping problems which are difficult to compute. Examples are roll motion and capsizing, slamming and water on deck. Linear seakeeping problems are only measured for research purposes to supply validation data for computational methods. In these cases many different frequencies can be measured at the same time. The measured data can then be decomposed (filtered) to obtain the reactions to the individual wave frequencies.

Seakeeping tests are expensive due to the long waiting periods between tests until the water has come to rest again. The waiting periods are especially long in conventional towing tanks. Also, the scope of the experiments is usually large as many parameters need to be varied, e.g. wave length, wave height, angle of encounter, ship speed, draught and trim, metacentric height, etc. Tests keep Froude similarity just as in resistance and propulsion tests. Gravity and inertia forces then correspond directly between model and full-scale ship. However, scale effects (errors due to the model scale) occur for forces which are due to viscosity, surface tension, compressibility of the water, or model elasticity. These effects are important, for example, for slamming pressure, water on deck, or sway, roll and yaw motions. However, in total, scale effects play a lesser role for seakeeping tests than for resistance and propulsion tests or maneuvering tests.

Seakeeping can also be measured on ships in normal operation or during special trial tests. Ship motions (with accelerometers and gyros) and sometimes also global and local loads (strain gauges), loss of speed, propeller rpm and torque are all measured. Recording the seaway is difficult in full-scale measurements. The options are:

1. No recording of actual seaway during trial; instead measurements of seaway over many years such that, for example, the expected maximum values during the lifetime of the ship can be extrapolated from the recorded distribution of long-term measured values (long-term measurement). The random variation of the actual seastate encountered by the ship introduces considerable inaccuracies for the predicted extreme values even if several years of measurements are available.

2. Computation of the seaway from the ship motions based on computed or model-test measured response amplitude operators for the motions. This allows only a rather rough estimate of the seaway. In following seas this method is hardly applicable. Nevertheless, averaging over, say, 10−100 half-hour measurements usually yields good estimates for the correlation of loads and seaway (medium-term measurement).
3. Parallel measurement of the seaway. Options are:
   - Using seastate measuring buoys (brought by the ship).
   - Performing the sea trials near a stationary seaway measuring installation.
   - Measuring the ship motions (by accelerometers) and the relative motion between water and ship (by pressure measurements at the hull or water level measurements using a special radar device); based on these data indirect determination of the absolute motion of the water surface is possible.
   - Measuring the wave spectrum (energy distribution over frequency and propagation direction) by evaluating radar signals reflected by the waves.
   - Computation or estimation of the seaway from the wind field before and during the experiments.
   - Estimation of significant wave height and period from 'experienced' seamen. This common practice is far too inaccurate: the correlation coefficient between measured (actual) and estimated wave period is typically <50%! This holds also if the estimates are used to derive statistical distributions. For most extreme values of interest the errors in the estimates do not cancel, but are rather concentrated around the extreme values.

4.3. Waves and Seaway

4.3.1. Airy Waves (Harmonic Waves of Small Amplitude)

Wind-induced seaways can be approximated by the superposition of regular waves of small wave height (elementary waves, Airy waves). Each elementary wave has a sinusoidal profile with an infinite number of wave troughs and wave crests (Fig. 4.1). The wave troughs and crests are perpendicular to the direction of wave propagation. Such elementary waves are an important building block for all computational methods for linear seakeeping problems. Steep regular waves can be computed by, for example, Stokes' theory or panel methods. However, the superposition principle no longer applies to these waves. Therefore they play virtually no role at all in the prediction of ship seakeeping and are of rather academic interest for naval architects. Unfortunately, in using the superposition principle for elementary waves, all properties of the seaway which are non-linear with wave steepness (= wave height/wave length) are lost.

These are, for example, the broader wave troughs and steeper wave crests, the higher celerity of steeper waves which results in a tendency to form wave groups in natural wind seas: groups of waves with low wave height are followed by groups of waves with larger wave heights.

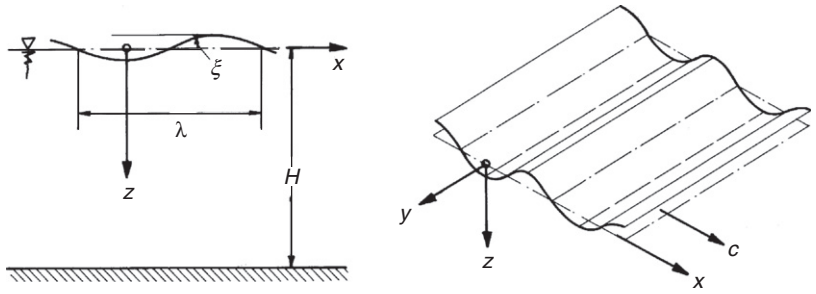

Figure 4.1:
Elementary waves

For ship seakeeping, the relevant waves are dominated by gravity effects. Surface tension, water compressibility and (for deep and moderately shallow water) viscosity can be neglected. Computations can then assume an ideal fluid (incompressible, inviscid) without surface tension. Consequently potential theory can be applied to describe the waves.

Generally, regular waves are described by a length parameter (wave length λ or wave number k) and a time parameter (wave period T or (circular) frequency ω). k and ω are defined as follows:

$$k = \frac{2\pi}{\lambda}; \quad \omega = \frac{2\pi}{T} \tag{4.1}$$

The celerity c denotes the speed of wave propagation, i.e. the speed of an individual wave crest or wave trough:

$$c = \frac{\lambda}{T} = \frac{\omega}{k} \tag{4.2}$$

For elementary waves, the following (dispersion) relation holds:

$$k = \frac{\omega^2}{g} \quad \text{on deep water} \tag{4.3}$$

$$k \tanh(kH) = \frac{\omega^2}{g} \quad \text{on finite depth} \tag{4.4}$$

$g = 9.81\ \text{m/s}^2$ and H is the water depth (Fig. 4.1).

The above equations can then be combined to give the following relations (for deep water):

$$c = \sqrt{\frac{g}{k}} = \frac{g}{\omega} = \sqrt{\frac{g\lambda}{2\pi}} = \frac{gT}{2\pi} \tag{4.5}$$

The potential ϕ of a wave traveling in the $+x$ direction is:

$$\phi = \mathrm{Re}(-ic\widehat{h}e^{-kz}\mathrm{e}^{i(\omega t-kx)}) \quad \text{for deep water} \tag{4.6}$$

$$\phi = \mathrm{Re}\left(\frac{-ic\widehat{h}}{\sinh(kH)}\cosh(k(z-H))\mathrm{e}^{i(\omega t-kx)}\right) \quad \text{for finite depth} \tag{4.7}$$

Re denotes the real part of a complex quantity; $i = \sqrt{-1}$; z as in Fig. 4.1; ^ denotes as usual a complex amplitude; $\widehat{h}$ = the complex amplitude of the wave. $h = |\widehat{h}|$ is the (real-valued) wave amplitude, i.e. half the wave height (from wave trough to wave crest). The real part of $\widehat{h}$ gives the distance of the wave trough from the calm-water level at time $t = 0$ at $x = 0$; the imaginary part gives the same value at ¼ period earlier. The deep-water formulae are applicable with errors of $< 0.5\%$ if the water depth is larger than half a wave length.

The velocity is obtained by differentiation of the potential, e.g. for deep water:

$$v_x = \frac{\partial\phi}{\partial x} = \phi_x = \mathrm{Re}(-\omega\widehat{h}\mathrm{e}^{-kz}\mathrm{e}^{i(\omega t-kx)}) \tag{4.8}$$

$$v_z = \frac{\partial\phi}{\partial z} = \phi_z = \mathrm{Re}(i\omega\widehat{h}\mathrm{e}^{-kz}\mathrm{e}^{i(\omega t-kx)}) \tag{4.9}$$

The complex amplitudes of the velocities have the same absolute value and a phase shift of 90°. A water particle thus follows a circular track or orbital motion (from Latin *orbis* = circle). In water of finite depth, the motion of a water particle follows an ellipse. The vertical axis of each ellipse decreases with depth until at the water bottom $z = H$ the motion is only in the horizontal direction.

If we excite a group of waves (not elementary waves, but, say, ten wave crests and troughs) in initially calm water we will notice that the front of the wave crests decay while at the end of the wave packet new wave crests are formed (Fig. 4.2). The wave packet thus moves slower than the wave crests, i.e. with a speed slower than celerity c, namely with group velocity c_{gr}:

$$c_{gr} = \frac{1}{2}c \quad \text{for deep water} \tag{4.10}$$

$$c_{gr} = c\left(\frac{1}{2} + \frac{kH}{\sinh(2kH)}\right) \quad \text{for finite depth} \tag{4.11}$$

The linearized Bernoulli equation

$$p + \rho\frac{\partial\phi}{\partial t} - \rho gz = p_0 \tag{4.12}$$

and the wave potential give the difference pressure to atmospheric pressure at a point below the water surface (for deep water):

$$p - p_0 = \rho gz - \rho g\,\mathrm{Re}\left(\widehat{h}\mathrm{e}^{-kz}\mathrm{e}^{i(\omega t-kx)}\right) \tag{4.13}$$

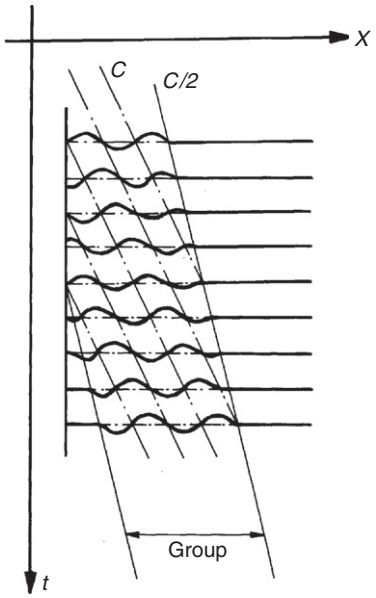

Figure 4.2:
Celerity and group velocity

p_0 is the atmospheric pressure, ρ the water density, and z the depth of the point below the calm-water surface. The first term represents the hydrostatic pressure in calm water. The second term represents the pressure change due to the wave. As with all wave effects, it decays exponentially with depth. The pressure gradient $\partial p/\partial z$ for the hydrostatic case is equal to the specific weight of the fluid and causes a buoyant lifting force on the immersed body that equals the weight of the displaced water. This lifting force changes in a wave! The lifting force is lower in a wave crest, higher in a wave trough. This is called the Smith effect.

The mechanical energy E per area of the water surface is composed of potential and kinetic energy. Let ζ be the momentary elevation of the free surface. Then the potential energy (per area) is:

$$E_{\text{pot}} = -\frac{\zeta}{2}\rho g(-\zeta) = \frac{1}{2}\rho g\zeta^2 \tag{4.14}$$

The potential energy is positive both in wave troughs and wave crests and oscillates in time and space between 0 and $\frac{1}{2}\rho g|\widehat{h}|^2$. The time average is

$$\overline{E}_{\text{pot}} = \frac{1}{4}\rho g|\widehat{h}|^2 \tag{4.15}$$

The kinetic energy per area is:

$$E_{\text{kin}} = \int_{\zeta}^{\infty} \frac{1}{2}\rho\left(v_x^2 + v_z^2\right)\ \mathrm{d}z = \int_{\zeta}^{\infty} \frac{1}{2}\rho\omega^2|\widehat{h}|^2 \mathrm{e}^{-2kz}\,\mathrm{d}z \approx \int_{0}^{\infty} \ldots\ \mathrm{d}z = \frac{1}{4}\rho g|\widehat{h}|^2 \tag{4.16}$$

Here Eqs. (4.8) and (4.9) have been used and in a linearization the wave elevation ζ was substituted by 0. The kinetic energy is constant in time and space. The time-averaged total energy per area for a deep-water wave is then:

$$\overline{E} = \frac{1}{2}\rho g|\widehat{h}|^2 \tag{4.17}$$

The average energy travels with c_{gr} in the same direction as the wave. For finite-depth water the average energy remains the same but the kinetic energy also oscillates in time and space.

The elementary wave was so far described in an earth-fixed coordinate system. In a reference system moving with ship speed V in the direction of the ship axis x_s under an angle of encounter μ (Fig. 4.3), the wave seems to change its frequency. The (circular) frequency experienced by the ship is denoted encounter frequency:

$$\omega_e = |\omega - kV\cos\mu| = \left|\omega - \frac{\omega^2 V}{g}\cos\mu\right| \tag{4.18}$$

Figure 4.4 illustrates this phenomenon. For course against the sea ($\mu > 90°$) the encounter frequency is higher than the incident wave frequency ω. For course with the sea ($\mu < 90°$) the encounter frequency is usually lower than the incident wave frequency ω. An exception is short following seas which are passed by the ship. The condition for the ship passing the waves is:

$$F_n > \frac{0.4}{\cos\mu}\sqrt{\frac{\lambda}{L}} \tag{4.19}$$

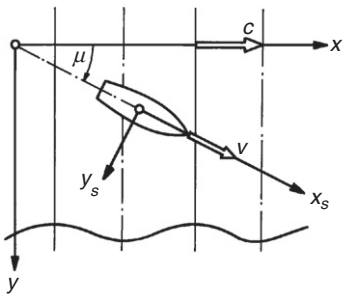

Figure 4.3:
Definition of angle of encounter

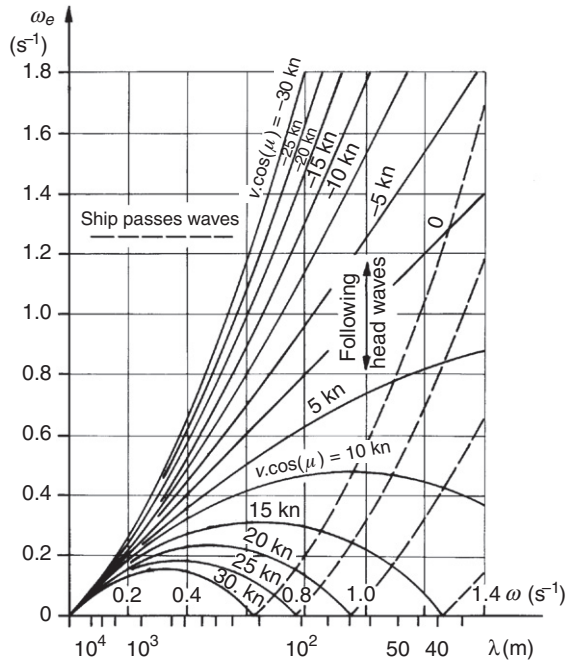

Figure 4.4:
Relation between wave frequency, wave length, and encounter frequency

An important parameter in this context is:

$$\tau = \frac{\omega_e V}{g} = \frac{\omega V}{g} - \left(\frac{\omega V}{g}\right)^2 \cos\mu \tag{4.20}$$

For following sea for cases with $\tau \cos\mu < 0.25$, for given speed V, encounter angle μ, and encounter frequency ω_e three possible ω values exist:

$$\omega_1 = \frac{g}{2V\cos\mu}(1 + \sqrt{1 + 4\tau\cos\mu}) \tag{4.21}$$

$$\omega_2 = \frac{g}{2V\cos\mu}(1 + \sqrt{1 - 4\tau\cos\mu}) \tag{4.22}$$

$$\omega_3 = \frac{g}{2V\cos\mu}(1 - \sqrt{1 - 4\tau\cos\mu}) \tag{4.23}$$

The potential of a deep-water wave in a coordinate system moving with ship speed is:

$$\phi = \mathrm{Re}(-ic\hat{h}\mathrm{e}^{-kz}\mathrm{e}^{-ik(x_s\cos\mu - y_s\sin\mu)}\mathrm{e}^{i\omega_e t}) \tag{4.24}$$

The above formulae for velocities and pressures can correspondingly be derived in the coordinate system moving with ship speed.

4.3.2. Natural Seaway

Wind-excited seaway can be approximated with good accuracy as the superposition of many elementary waves of different wave lengths and propagation directions. The phase shifts between these elementary waves change with time and location and are taken as random quantities for the origin and time $t = 0$. The randomness of the phases − which corresponds to the randomness (irregularity) of the natural seaway − means that only statistical statements can be made, e.g. what the probability is that the wave height exceeds a given limit.

The initial assumptions are:

1. The seaway is stationary, i.e. its statistical properties (e.g. average wave height, average wave period, etc.) do not change within the considered time frame.
2. The seaway is not too steep so that linearized equations are still accurate enough. Then any linear superposition of two or more waves with the same or differing frequency or propagation direction will again be a possible form of the water surface.

Only those seaway properties which do not change for small variations of the registration location or the registration time are of interest for ship seakeeping. The procedure to obtain these properties is as follows. Assume we have a record of the wave elevation $\zeta(t)$ at a given point for the time interval $t = 0$ to T. Then ζ is decomposed in a Fourier analysis, i.e. the complex constants $\widehat{A}_j$ are determined in a finite series:

$$\zeta(t) = A_0 + \sum_{j=1}^{J} \mathrm{Re}(\widehat{A}_j \, \mathrm{e}^{i\omega_j t}) \quad \text{with } \omega_j = j\Delta\omega, \ \Delta\omega = 2\pi/T \tag{4.25}$$

The average wave elevation A_0 is of no interest here. The phase angle ε_j of the complex amplitudes $\widehat{A}_j = |\widehat{A}_j|\mathrm{e}^{i\varepsilon_j}$ would be different at a different (nearby) location and is therefore also of no interest here. The absolute value of $\widehat{A}_j$ depends on the registration time T. Only the sea spectrum remains as constant and of interest in the above sense:

$$S_\zeta(\omega_j) = \frac{\text{Average value of } \ |\widehat{A}_j|^2}{2\Delta\omega_j} \tag{4.26}$$

The averaging can be done:

- over many records of statistically equivalent seaways (e.g. at various locations spaced by a few kilometers at the same time), or
- over many records of time intervals of the total registration time T, or
- over several (10 to 30) 'neighboring' $|\widehat{A}_j|^2$ (preferred choice in practice); e.g. for $j = 1$ to 10, 11 to 20, 21 to 30 etc., an average $|\widehat{A}_j|^2$ can be found as the arithmetic average of ten $|\widehat{A}_j|^2$ in each case.

The ω_j in the argument of the sea spectrum S_ζ is the (circular) frequency (in the last case the average frequency) on which the average is based.

The wave energy per horizontal area in an elementary wave is:

$$\overline{E} = \frac{1}{2}\rho g|\widehat{A}|^2 \tag{4.27}$$

$\rho g S_\zeta$ is thus the average seaway energy per frequency interval and area. Therefore S_ζ is also called the energy spectrum of a seaway. It describes the distribution of wave energy over the frequency ω. Its dimension is, e.g., $m^2 \cdot s$.

The spectrum can be used to reconstruct the time function $\zeta(t)$ given in Eq. (4.25):

$$\zeta(t) = \sum_{j=1}^{J} \sqrt{2S_\zeta(\omega_j)\Delta\omega_j} \cdot \cos(\omega_j t + \varepsilon_j) \tag{4.28}$$

(Instead of Re $e^{i\alpha}$ we simply write here cos α.) We substituted here $|\widehat{A}_j|^2$ by its average value; this usually has no significant effect. As the phase angle information is no longer contained in the spectrum (and we usually only have the spectrum information to reconstruct a seaway) the phase angles ε_j are chosen as random quantities equally distributed in the interval $[0, 2\pi]$. This creates various functions $\zeta(t)$ depending on the actual choice of ε_j, but all these functions have the same spectrum, i.e. the same characteristic (non-random) properties as the original seaway.

If all phase angles are chosen as zero the extremely unlikely (but not impossible) case results that all elementary waves have a wave trough at the considered location at time $t = 0$. The number of terms in the sum for $\zeta(t)$ in the above equation is taken as infinite in theoretical derivations. In practical simulations, usually 30 to 100 terms are taken.

Each elementary wave in a Fourier decomposition of natural seaway depends on time and space. The superposition of many elementary waves all propagating in the x direction, but

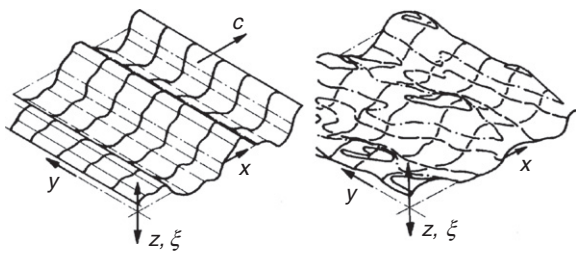

Figure 4.5:
Long-crested (left) and short-crested (right) seaways

having different frequencies, yields long-crested seaways as depicted in Fig. 4.5 (left).
Long-crested seaway is described by:

$$\zeta(t) = \sum_{j=1}^{J} \sqrt{2S_\zeta(\omega_j)\Delta\omega_j} \cdot \cos(\omega_j t + k_j x + \varepsilon_j) \tag{4.29}$$

$k_j = \omega_j/g$ is the wave number corresponding to frequency ω_j.
Short-crested seaway (Fig. 4.5 (right)) is a better approximation to wind-excited seaway. Short-crested seaway is described if the wave energy is distributed not only over frequency, but also over wave propagation direction μ. The corresponding description is:

$$\zeta(t) = \sum_{j=1}^{J} \sum_{l=1}^{L} \sqrt{2S_\zeta(\omega_j, \mu_l)\Delta\omega_j\Delta\mu_l} \cdot \cos[\omega_j t - k_j(x \cos \mu_l - \sin \mu_l) + \varepsilon_{jl}] \tag{4.30}$$

$S_\zeta(\omega_j,\mu_l)$ is the directional or two-dimensional spectrum as opposed to the one-dimensional spectrum $S_\zeta(\omega_j)$.

At a ship, the wave elevation oscillates in a regular wave with encounter frequency ω_e. The encounter spectrum $S_e(\omega_e)$ describes the distribution of the wave energy in a seaway over ω_e instead of ω. The energy must be independent of the reference system:

$$S_\zeta(\omega) \cdot |\Delta\omega| = S_{\zeta e}(\omega_e) \cdot |\Delta\omega_e| \tag{4.31}$$

This yields:

$$S_{\zeta e}(\omega_e) = \frac{S_\zeta(\omega)}{\mathrm{d}\omega_e/\mathrm{d}\omega} = \frac{S_\zeta(\omega)}{\left|1 - \dfrac{2\omega}{g} V \cos \mu\right|} \tag{4.32}$$

If several ω result in the same ω_e the contributions of all three frequencies are added on the r.h.s. of this equation (Fig. 4.6). Correspondingly an encounter directional spectrum can also be determined. Because of the several possible contributions on the r.h.s. and the singularity at S_e – where the denominator on the r.h.s. in the above equation becomes zero – the encounter spectrum is not used in seakeeping computations. However, it is needed for the analysis of data if these were measured from a ship with forward speed.

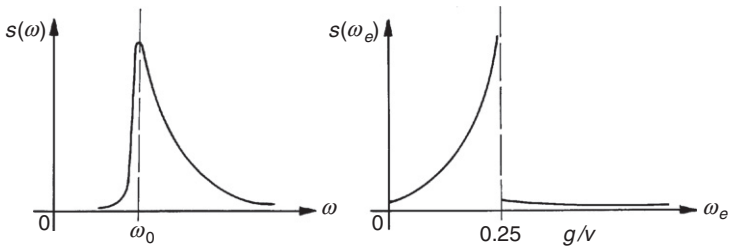

Figure 4.6:
Sea spectrum and corresponding encounter spectrum

4.3.3. Wind and Seaway

We distinguish between swell and wind sea. Swell waves have a celerity higher than the present wind speed (e.g. measured in 10 m height above mean sea level; only the component in the wave propagation direction is considered). Swell has been excited originally by some stronger winds at some other location and propagates without significant damping or excitation until it is damped in shallow-water regions or excited again to wind sea in stronger winds. By definition, wind sea has celerity less or equal to the wind speed. Due to the gustiness of wind and other factors, the distinction between swell and wind sea is not sharp.

Swell, sometimes also wind sea (for winds changing rapidly in time or space), can change the form of the spectrum considerably. On the other hand, a rather uniform form of a wind sea spectrum is achieved within ½ to 1 hour if the wind is constant in time and space. The relevant area in this context extends over a distance of (½ to 1 hour)/group velocity of waves in a downwind direction. In the following, we will consider only spectra developed in constant wind. The spectrum parameters, especially wave height and period, converge only after many hours or several days to constant values. The form of the spectrum is determined by the physical processes of:

- wave generation (e.g. the wind resistance of wave crests);
- dissipation (wave-breaking; in shallow water also friction at the ocean bottom);
- convection (transport of wave energy with group velocity);
- non-linear interaction between waves of different frequencies and direction.

The directional spectrum is described as the product of a one-dimensional spectrum $S_\zeta(\omega)$ with a function f. f describes the distribution of the wave energy over the propagation direction μ assumed to be symmetrical to a main propagation direction μ_0:

$$S_\zeta(\omega, \mu) = S_\zeta(\omega) \cdot f(\mu - \mu_0) \tag{4.33}$$

Söding and Bertram (1998) give a more modern form than the often cited Pierson–Moskowitz and JONSWAP spectra. The older spectra assume a stronger decay of the wave energy at higher frequencies (proportional to ω^{-5}, while more recent measurements indicate decay proportional to ω^{-4}).

The one-dimensional spectrum $S_\zeta(\omega)$ must be zero for small frequencies (where the wave celerity is much higher than the wind speed) and converge to zero for high frequencies, because high frequency means short waves, which in turn can only have small height as the wave steepness before breaking is limited. In between, there must be a maximum. The (circular) frequency where the spectrum assumes its maximum is called modal frequency or peak frequency ω_p. The function $S_\zeta(\omega)$ contains as an important parameter U_c/c_p. U_c is the component of the wind velocity in the main direction of wave propagation, measured in 10 m

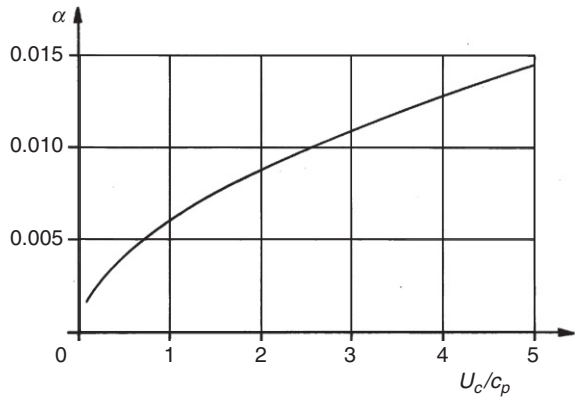

Figure 4.7:
Spectrum factor

height. c_p is the celerity of elementary waves of frequency ω_p. c_p is computed using the formula $c_p = g/\omega_p$ which is valid for elementary waves. In reality, waves of frequency ω_p travel some 5−10% faster due to their larger steepness. The ratio U_c/c_p usually lies between 1 (fully developed seaway) and 5 (strongly increasing seaway).

$S_\zeta(\omega)$ is written as the product of three factors:

- an initial factor $\alpha g^2/\omega_p^5$
- a 'base form' containing the ω dependency (corresponding to the Pierson−Moskowitz spectrum widely used previously)
- a peak enhancement factor γ^Γ independent of U_c/c_p:

$$S_\zeta(\omega) = \frac{\alpha g^2}{\omega_p^5} \cdot \left(\frac{\omega_p}{\omega}\right)^4 \exp\left[-\left(\frac{\omega_p}{\omega}\right)^4\right] \cdot \gamma^\Gamma \tag{4.34}$$

with $\alpha = 0.006(U_c/c_p)^{0.55}$.

Figure 4.7 illustrates α, Fig. 4.8 the base form, and Fig. 4.9 the peak enhancement for three representative values of U_c/c_p. The peak enhancement makes the maximum of the spectrum very pointed for a not fully developed seaway ($U_c/c_p > 1$), while fully developed seaways feature broader and less-pronounced maxima. γ describes the maximum of the peak enhancement over ω. It occurs at ω_p and increases the 'base form' by a factor of:

$$\gamma = 1.7 + \max[0.6 \log_{10}(U_c/c_p)] \tag{4.35}$$

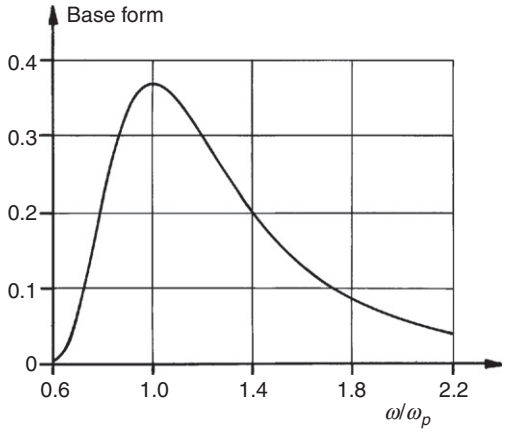

Figure 4.8:
Spectrum base form

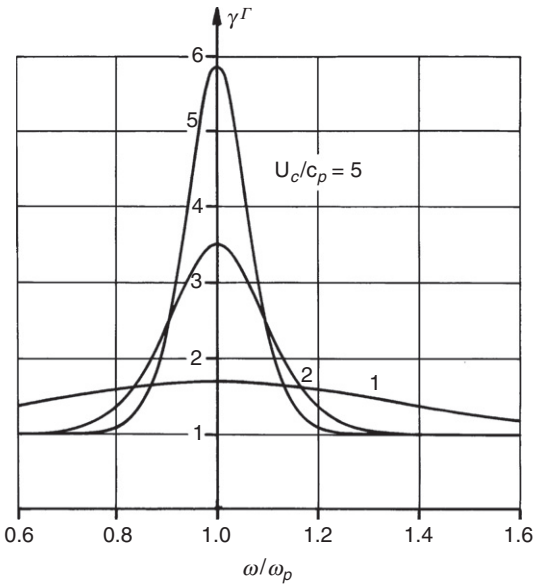

Figure 4.9:
Peak enhancement factor

Γ describes how the enhancement factor decays left and right of the model frequency ω_p; for this purpose a formula corresponding to a normal (Gaussian) distribution is chosen (but without a forefactor; thus the maximum of Γ is 1):

$$\Gamma = \exp\left(-\frac{(\omega/\omega_p - 1)^2}{2\sigma^2}\right) \quad \text{with} \quad \sigma = 0.08\left[1 + \frac{4}{(U_c/c_p)^3}\right] \tag{4.36}$$

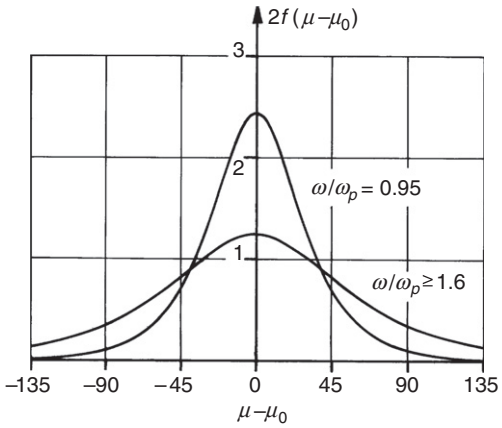

Figure 4.10:
Angular distribution of seaway energy

The distribution of the wave energy over the propagation direction $f(\mu - \mu_0)$ is independent of U_c/c_p. Instead, it depends on the non-dimensional frequency ω/ω_p:

$$f(\mu - \mu_0) = \frac{0.5\beta}{\cosh^2[\beta(\mu - \mu_0]} \text{ with} \tag{4.37}$$

$$\beta = \max\left(1.24, 2.61(\omega/\omega_p)^{1.3}\right) \quad \text{for } \omega/\omega_p < 0.95 \tag{4.38}$$

$$\beta = \max\left(1.24, 2.28(\omega/\omega_p)^{-1.3}\right) \quad \text{for } \omega/\omega_p \geq 0.95 \tag{4.39}$$

Figure 4.10 illustrates $f(\mu - \mu_0)$. Figure 4.11 illustrates $\beta(\omega/\omega_p)$.

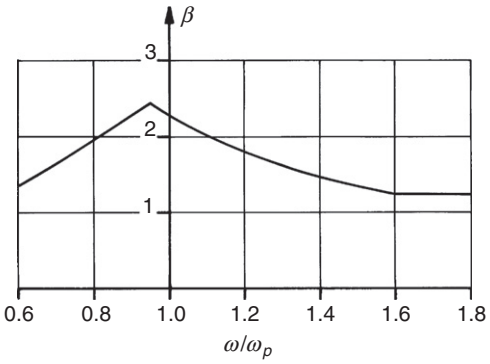

Figure 4.11:
Angular spreading β

Since short waves adapt more quickly to the wind than long waves, a changing wind direction results in a frequency-dependent main propagation direction μ_0. Frequency-dependent μ_0 are also observed for oblique offshore wind near the coast. The wave propagation direction here is more parallel to the coast than the wind direction, because this corresponds to a longer fetch.

The (only statistically defined) wave steepness = wave height/wave length does not depend strongly on the wind velocity, U_c/c_p, or ω/ω_p. The wave steepness is so large that the celerity deviates noticeably from the theoretical values for elementary waves (of small amplitude) as described above. Also, the average shape of the wave profiles deviates noticeably from the assumed sinusoidal wave forms of elementary waves. However, non-linear effects in the waves are usually much weaker than the non-linear effects of ship seakeeping in the seaway.

The significant wave height $H_{1/3}$ of a seaway is defined as the mean of the top third of all waves, measured from wave crest to wave trough. $H_{1/3}$ is related to the area m_0 under the sea spectrum:

$$H_{1/3} = 4\sqrt{m_0} \quad \text{with } m_0 = \int_0^\infty \int_0^{2\pi} S_\zeta(\omega, \mu)\, \mathrm{d}\mu\, \mathrm{d}\omega \tag{4.40}$$

For the above given wind sea spectrum, $H_{1/3}$ can be approximated by:

$$H_{1/3} = 0.21 \frac{U_c^2}{g} \left(\frac{U_c}{c_p} \right)^{-1.65} \tag{4.41}$$

The modal period is:

$$T_p = 2\pi/\omega_p \tag{4.42}$$

The periods T_1 and T_2, which were traditionally popular to describe the seaway, are much shorter than the modal period. T_1 corresponds to the frequency ω where the area under the spectrum has its center. T_2 is the average period of upward zero crossings.

If we assume that water is initially calm and then a constant wind blows for a duration t and over a distance x, the seaway parameter U_c/c_p becomes approximately:

$$\frac{U_c}{c_p} = \max(1, 18\xi^{-3/10}, 110\theta^{-3/7}) \tag{4.43}$$

ξ is the non-dimensional fetch x, θ the non-dimensional wind duration t:

$$\xi = gx/U_c^2; \quad \theta = gt/U_c \tag{4.44}$$

The fetch is to be taken upwind from the point where the seaway is considered, but of course at most to the shore. In reality, there is no sudden and then constant wind. But the seakeeping

Table 4.1: Sea spectra for various wind duration times for $U_c = 20$ m/s

Quantity	Case 1	Case 2	Case 3
Assumed wind duration time t	5 h	20 h	50 h
Non-dimensional duration time θ	8830	35000	88000
Maturity parameter U_c/c_p	2.24	1.24	1
Significant wave height $H_{1/3}$	2.26 m	6.00 m	8.56 m
$\omega_p = g/c_p = g/U_c \cdot U_c/c_p$	1.10 Hz	0.61 Hz	0.49 Hz
Modal period $2\pi/\omega_p$	5.7 s	10.3 s	12.8 s

parameters are not very sensitive towards x and t. Therefore it is possible to estimate the seaway with practical accuracy in most cases when the wind field is given.

Table 4.1 shows how the above formulae estimate the seaway parameters $H_{1/3}$ and T_p for various assumed wind durations t for an exemplary wind velocity $U_c = 20$ m/s. The fetch x was assumed to be so large that the center term in the 'max'-bracket in the above formula for U_c/c_p is always smaller than one of the other two terms. That is, the seaway is not fetch-limited, but either time-limited (for $110\theta^{-3/7} > 1$) or fully developed.

Figure 4.12 shows wind sea spectra for $U_c = 20$ m/s for various fetch values. Figure 4.13 shows the relation between wave period T_p and significant wave height $H_{1/3}$ for various values of U_c/c_p. c_p (lower scale) and U_c/c_p together yield the wind velocity U_c that has excited the wind

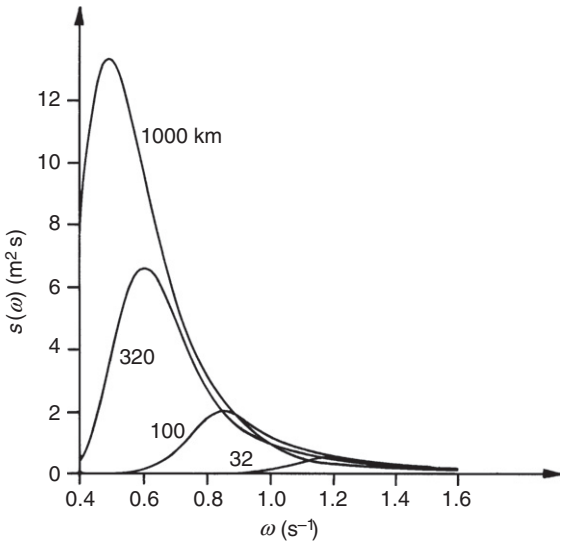

Figure 4.12:
Wind sea spectra for $U_c = 20$ m/s for various fetch values

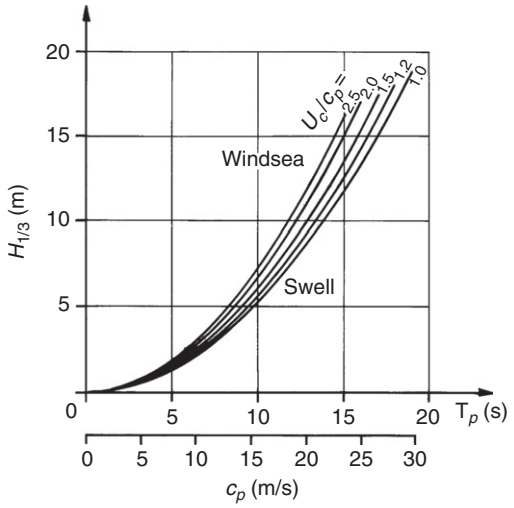

Figure 4.13:
Correlation between significant wave height $H_{1/3}$, modal period T_p, wind speed U_c, and wave celerity at modal frequency c_p

sea characterized by $H_{1/3}$ and T_p. For swell, we can assume $U_c \approx c_p$. Figure 4.14 shows the relation between various seaway parameters, the 'wind force' and the wind velocity U_c.

Programs to compute the given wind sea spectrum from either U_c, t, and x or $H_{1/3}$ and T_p are given by Söding (1997).

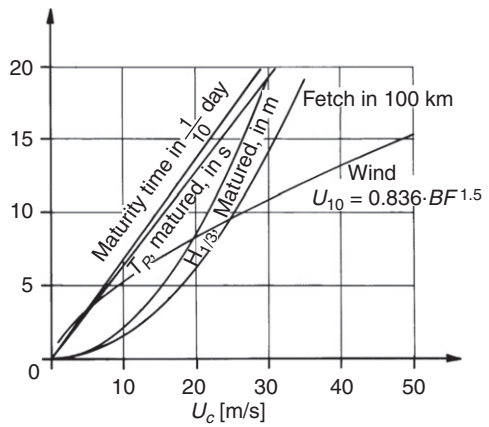

Figure 4.14:
Key wind sea parameters depending on the wind speed U_c (component in wave propagation direction in 10 m height)

Table 4.2: Relative occurrence · 10^6 of combinations of $H_{1/3}$ and T_1 in the North Atlantic

T_1 (s)			$H_{1/3}$ (m)															
from	*to*	*FCUM*	*0.5*	*1.5*	*2.5*	*3.5*	*4.5*	*5.5*	*6.5*	*7.5*	*8.5*	*9.5*	*11.0*	*13.0*	*15.0*	*17.0*	*19.0*	*21.0*	*24.0*
1.9	3.1	0.2	2040	0	0	0	0	0	0	0	0	0	0	0	0	0	0	0	0
3.1	4.3	0.6	2343	1324	0	0	0	0	0	0	0	0	0	0	0	0	0	0	0
4.3	5.3	5.3	21165	25562	306	0	0	0	0	0	0	0	0	0	0	0	0	0	0
5.3	6.2	14.3	17770	51668	20543	308	0	0	0	0	0	0	0	0	0	0	0	0	0
6.2	7.1	26.4	14666	38973	58152	8922	0	0	0	0	0	0	0	0	0	0	0	0	0
7.1	7.9	41.6	15234	29453	52102	49055	6093	304	0	0	0	0	0	0	0	0	0	0	0
7.9	9.0	57.0	9918	21472	33742	43660	36809	7464	715	0	0	0	0	0	0	0	0	0	0
9.0	10.1	75.9	7894	21221	26655	37214	39675	36189	17120	2768	307	0	0	0	0	0	0	0	0
10.1	11.1	85.4	3062	8167	11945	14497	15621	15314	13579	9188	3369	714	0	0	0	0	0	0	0
11.1	12.1	91.3	1672	4094	6034	7374	8208	8467	8121	6955	4845	2120	822	0	0	0	0	0	0
12.1	13.2	95.2	981	2185	3140	3986	4659	4948	4947	4726	4117	3062	2318	215	0	0	0	0	0
13.2	14.6	97.7	547	1038	1527	2122	2418	2633	2788	2754	2632	2385	3043	784	78	0	0	0	0
14.6	16.4	99.1	269	412	719	942	1069	1259	1312	1374	1358	1325	2246	1303	378	44	0	0	0
16.4	18.6	99.8	110	124	290	314	424	451	516	534	559	557	1072	908	544	197	43	3	0
18.6	21.0	100.0	32	32	71	86	106	126	132	151	154	162	327	314	268	187	86	27	5
		FCUM	9.8	30.3	51.9	68.7	80.2	87.9	92.9	95.7	97.4	98.5	99.5	99.8	99.9	100.0	100.0	100.0	100.0

4.3.4. Wave Climate

Predictions of maximum loads, load spectra for fatigue strength analyses, etc. require distributions of the significant seaway properties in individual ocean areas. The best sources for such statistics are computations of the seaway based on measured wind fields. ANEP-II (1983) gives such statistical data extensively for North Atlantic, North Sea, Baltic Sea, Mediterranean Sea, and Black Sea. Based on these data, Germanischer Lloyd derived distributions for $H_{1/3}$ and T_1 for all of the Atlantic between 50 and 60 longitudinal and the western Atlantic between 40 and 50 longitudinal (Table 4.2). The table is based on data for a period of 10 years. T_1 is the period corresponding to the center of gravity of the area under the sea spectrum. The modal period for this table is:

$$T_p = T_1/0.77$$

The values in the table give 10^6 the time share when T_1 was in the given time interval and $H_{1/3}$ in the interval denoted by its mean value, at an arbitrary point in the sea area. FCUM denotes the cumulated share in per cent. Similar tables can be derived from ANEP-II and other publications for special seaway directions, seasons, and other ocean areas.

Table 4.2 can also be used to approximate other ocean areas by comparing the wind field in the North Atlantic with the wind field in another ocean area, using data of Blendermann (1998), and employing the relation between wind and sea as given in the previous chapter.

4.4. Numerical Prediction of Ship Seakeeping

4.4.1. Overview of Computational Methods

If the effect of the wave amplitude on the ship seakeeping is significantly non-linear, there is little sense in investigating the ship in elementary waves, since these waves do not appear in

nature and the non-linear reaction of the ship in natural seaways cannot be deduced from the reaction in elementary waves. In these non-linear cases, simulation in the time domain is the appropriate tool.

If the non-linearity is weak or moderate the seakeeping properties of a ship in natural seaways can be approximated by superposition of the reactions in elementary waves of different frequency and direction. In these cases, the accuracy can be enhanced by introducing some relatively simple corrections of the purely linear computations to account for force contributions depending quadratically on the water velocity or considering the time-dependent change of position and wetted surface of the ship, for example. Even if iterative corrections are applied the basic computations of the ship seakeeping is still based on its reaction in elementary waves, expressed by complex amplitudes of the ship reactions. The time dependency is then always assumed to be harmonic, i.e. sinusoidal.

For flows involving strong non-linearities, particularly breaking waves or green water on deck, free-surface RANSE simulations are the most appropriate tool. Such simulations have entered industry practice to an increasing extent since the year 2000.

In practice, potential flow solvers still dominate in seakeeping predictions. The most frequent application is the computation of the linear seakeeping properties of a ship in elementary waves. In addition to the assumption for Euler solvers potential flow assumes that the flow is irrotational. This is no major loss in the physical model, because rotation is created by the water adhering to the hull and this information is already lost in the Euler flow model. Relevant for practical applications is that potential flow solvers are much faster than Euler and RANSE solvers, because potential flows have to solve only one linear differential equation instead of four non-linear coupled differential equations. Also, potential flow solvers are usually based on boundary element methods and need only to discretize the boundaries of the domain, not the whole fluid space. This reduces the effort in grid generation considerably. On the other hand, potential flow methods require a simple, continuous free surface. Flows involving breaking waves and splashes cannot be analyzed properly by potential flow methods.

In reality, viscosity is significant in seakeeping, especially if the boundary layer separates periodically from the hull. This is definitely the case for roll and yaw motions. In practice, empirical corrections are introduced. Also, for flow separation at sharp edges in the aftbody (e.g. vertical sterns, rudder, or transoms) a Kutta condition is usually employed to enforce a smooth detachment of the flow from the relevant edge.

The theoretical basics and boundary conditions of linear potential methods for ship seakeeping are treated extensively in the literature, e.g. by Newman (1978). Therefore, we can limit ourselves here to a description of the fundamental results important to the naval architect.

The ship flow in elementary waves is described in a coordinate system moving with ship speed in the x direction, but not following its periodic motions. The derivatives of the potential give the

velocity of water relative to such a coordinate system. The total velocity potential is decomposed:

$$\phi^t = (-Vx + \phi^s) + (\phi^w + \phi^I) \tag{4.45}$$

with
ϕ^t potential of total flow
$-Vx$ potential of (downstream) uniform flow with ship speed V
ϕ^s potential of the steady flow disturbance
ϕ^w potential of the undisturbed wave as given at the end of Section 4.3.1
ϕ^I remaining unsteady potential.

The first parenthesis describes the steady (time-independent) flow, the second parenthesis the periodic flow due to sea waves. The potentials can be superimposed, since the fundamental field equation (Laplace equation, describing continuity of mass) is linear with respect to ϕ^t:

$$\Delta\phi^t = \left(\frac{\partial^2}{\partial x^2} + \frac{\partial^2}{\partial y^2} + \frac{\partial^2}{\partial z^2}\right)\phi^t \tag{4.46}$$

Various approximations can be used for ϕ^s and ϕ^I which affect computational effort and accuracy of results. The most important linear methods can be classified as follows:

- *Strip method.* Strip methods are the standard tool for ship seakeeping computations. They omit ϕ^s completely and approximate ϕ^I in each strip $x =$ constant, independently of the other strips. Thus in essence the three-dimensional problem is reduced to a set (e.g. typically 10−30) of two-dimensional boundary value problems. This also requires a simplification of the actual free surface condition. The method originated in the late 1950s with the work of Korvin-Kroukovsky and Jacobs. Most of today's strip methods are variations of the strip method proposed by Salvesen, Tuck, and Faltinsen (1970). These are sometimes also called STF strip methods where the first letter of each author is taken to form the abbreviation. The two-dimensional problem for each strip can be solved analytically or by panel methods, which are the two-dimensional equivalents of the three-dimensional methods described below. The analytical approaches use conform mapping to transform semicircles to cross-sections resembling ship sections (Lewis sections). Although this transformation is limited and, for example, submerged bulbous bow sections cannot be represented in satisfactory approximation, this approach still yields for many ships results of similar quality as strip methods based on panel methods (close-fit approach). A close-fit approach (panel method) to solve the two-dimensional problem is described on the website. Strip methods are − despite inherent theoretical shortcomings − fast, cheap, and for most problems sufficiently accurate. However, this depends on many details. Insufficient accuracy of strip methods often cited in the literature is often due to the particular implementation of a code and not due to the strip method in principle. But, at least in their conventional form, strip methods fail (as do most other computational methods) for waves

shorter than perhaps one-third of the ship length. Therefore, the added resistance in short waves (being considerable for ships with a blunt waterline) can also only be estimated by strip methods if empirical corrections are introduced. Section 4.4.2 describes a linear strip method in more detail.

- *Unified theory.* Newman (1978) and Sclavounos developed at the MIT the 'unified theory' for slender bodies. Kashiwagi (1997) describes more recent developments of this theory. In essence, the theory uses the slenderness of the ship hull to justify a two-dimensional approach in the near field which is coupled to a three-dimensional flow in the far field. The far-field flow is generated by distributing singularities along the centerline of the ship. This approach is theoretically applicable to all frequencies, hence 'unified'. Despite its better theoretical foundation, unified theories failed to give significantly and consistently better results than strip theories for real ship geometries. The method therefore failed to be accepted in practice.
- *'High-speed strip theory' (HSST).* Several authors have contributed to the high-speed strip theory after the initial work of Chapman (1975). A review of work since then can be found in Kashiwagi (1997). HSST usually computes the ship motions in an elementary wave using linear potential theory. The method is often called the $2.5d$ or $2d+t$ method, since it considers the effect of upstream sections on the flow at a point x, but not the effect of downstream sections. Starting at the bow, the flow problem is solved for individual strips (sections) $x =$ constant. The boundary conditions at the free surface and the hull (strip contour) are used to determine the wave elevation and the velocity potential at the free surface and the hull. Derivatives in the longitudinal direction are computed as numerical differences to the upstream strip which has been computed in the previous step. The computation marches downstream from strip to strip and ends at the stern resp. just before the transom. HSST is the appropriate tool for fast ships with Froude numbers $F_n > 0.4$. For lower Froude numbers, it is inappropriate.
- *Green function method (GFM).* ISSC (1994) gives a literature review of these methods. GFM distributes panels on the average wetted surface (usually for calm-water floating position neglecting dynamical trim and sinkage and the steady wave profile) or on a slightly submerged surface inside the hull. The velocity potential of each panel (Green function) fulfills automatically the Laplace equation, the radiation condition (waves propagate in the right direction) and a simplified free-surface condition (omitting the ϕ^s completely). The unknown (either source strength or potential) is determined for each element by solving a linear system of equations such that for each panel at one point the no-penetration condition on the hull (zero normal velocity) is fulfilled. The various methods differ primarily in the way the Green function is computed. This involves the numerical evaluation of complicated integrals from 0 to ∞ with highly oscillating integrands. Some GFM approaches formulate the boundary conditions on the ship under consideration of the forward speed, but evaluate the Green function only at zero speed. This saves a lot of computational effort, but cannot be justified physically and it is not

recommended. As an alternative to the solution in the frequency domain (for excitation by elementary waves), GFM may also be formulated in the time domain (for impulsive excitation). This avoids the evaluation of highly oscillating integrands, but introduces other difficulties related to the proper treatment of time history of the flow in so-called convolution integrals. Both frequency and time domain solutions can be superimposed to give the response to arbitrary excitation, e.g. by natural seaway, assuming that the problem is linear. All GFMs are fundamentally restricted to simplifications in the treatment of ϕ^s. Usually ϕ^s is completely omitted, which is questionable for usual ship hulls. It will introduce, especially in the bow region, larger errors in predicting local pressures.

- *Rankine singularity method (RSM).* Bertram and Yasukawa (1996) give an extensive overview of these methods covering both frequency and time domains. RSMs, in principle, capture ϕ^s completely and also more complicated boundary conditions on the free surface and the hull. In summary, they offer the option for the best approximation of the seakeeping problem within potential theory. This comes at a price. Both ship hull and the free surface in the near field around the ship have to be discretized by panels. Capturing all waves while avoiding unphysical reflections of the waves at the outer (artificial) boundary of the computational domain poses the main problem for RSMs. Since the early 1990s, various RSMs for ship seakeeping have been developed. By the end of the 1990s, the time-domain SWAN code (SWAN = Ship Wave ANalysis) of MIT was the first such code to be used commercially.
- *Combined RSM−GFM approach.* GFMs are fundamentally limited in capturing the physics when the steady flow differs considerably from uniform flow, i.e. in the near field. RSMs have fundamental problems in capturing the radiation condition for low τ values. Both methods can be combined to overcome the individual shortcomings and to combine their strengths. This is the idea behind combined approaches. These are described as 'Combined Boundary Integral Equation Methods' by the Japanese, and as 'hybrid methods' by Americans. Initially only hybrid methods were used which matched near-field RSM solutions directly to far-field GFM solutions by introducing vertical control surfaces at the outer boundary of the near field. The solutions are matched by requiring that the potential and its normal derivative are continuous at the control surface between near field and far field. In principle methods with overlapping regions also appear possible.

4.4.2. Strip Method

This section presents the most important formulae for a linear frequency-domain strip method for slender ships in elementary waves. The formulae will be given without derivation. For a more extensive coverage of the theoretical background, the reader is referred to Newman (1978).

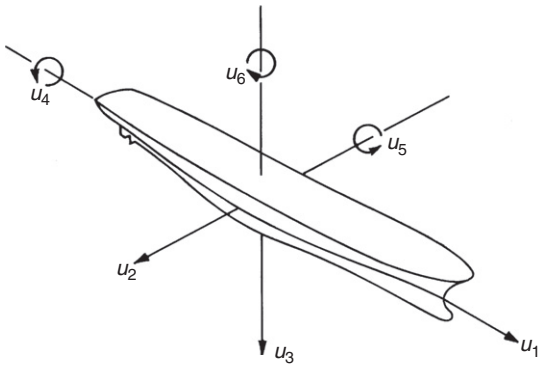

Figure 4.15:
Six degrees of freedom for motions

Two coordinate systems are used:

- The ship-fixed system x, y, z, with axes pointing from amidships forward, to starboard and downwards. In this system, the ship's center of gravity is time-independent x_g, y_g, z_g.
- The inertial system ξ, η, ζ. This system follows the steady forward motion of the ship with speed V and coincides in the time average with the ship-fixed system.

The main purpose of the strip method is to compute the ship's rigid-body motions, i.e. the three translations of the origin of ship-fixed system in the ξ, η, ζ direction and the three rotations around these axes. We denote (Fig. 4.15):

u_1	surge	u_4	roll
u_2	sway	u_5	pitch
u_3	heave	u_6	yaw

The motions are combined in a six-component vector $\overrightarrow{u}$. The forces and moments acting on the ship are similarly combined in a six-component vector $\overrightarrow{F}$. $\overrightarrow{u}$ and $\overrightarrow{F}$ are harmonic functions of time t oscillating with encounter frequency ω_e:

$$\overrightarrow{F} = \mathrm{Re}(\widehat{\overrightarrow{F}} e^{i\omega_e t}) \text{ and } \overrightarrow{u} = \mathrm{Re}(\widehat{\overrightarrow{u}} e^{i\omega_e t}) \tag{4.47}$$

The fundamental equation of motion is derived from $\overrightarrow{F} = M \cdot \ddot{\overrightarrow{u}}$:

$$[-\omega_e^2(M + A) + i\omega_e N + S]\ \widehat{\overrightarrow{u}} = \widehat{\overrightarrow{F}_e} \tag{4.48}$$

Here M, A, N, and S are real-valued 6×6 matrices. For mass distribution symmetrical to $y = 0$ the mass matrix M is:

$$M = \begin{bmatrix} m & 0 & 0 & 0 & mz_g & 0 \\ 0 & m & 0 & -mz_g & 0 & mx_g \\ 0 & 0 & m & 0 & -mx_g & 0 \\ 0 & -mz_g & 0 & \theta_{xx} & 0 & -\theta_{xz} \\ mz_g & 0 & -mx_g & 0 & \theta_{yy} & 0 \\ 0 & mx_g & 0 & -\theta_{xz} & 0 & \theta_{zz} \end{bmatrix} \tag{4.49}$$

The mass moments of inertia θ are related to the origin of the ship-fixed coordinate system:

$$\theta_{xx} = \int (y^2 + z^2)\, \mathrm{d}m\,; \quad \theta_{xz} = \int xz\, \mathrm{d}m\,; \text{ etc.} \tag{4.50}$$

If we neglect contributions from a dry transom stern and other hydrodynamic forces due to the forward speed of the ship, the restoring forces matrix S is:

$$S = \begin{bmatrix} 0 & 0 & 0 & 0 & 0 & 0 \\ 0 & 0 & 0 & 0 & 0 & 0 \\ 0 & 0 & \rho g A_w & 0 & -\rho g A_w x_w & 0 \\ 0 & 0 & 0 & gm\overline{GM} & 0 & 0 \\ 0 & 0 & -\rho g A_w x_w & 0 & gm\overline{GM}_L & 0 \\ 0 & 0 & 0 & 0 & 0 & \theta_{zz}\omega_g^2 \end{bmatrix} \tag{4.51}$$

Here A_w is the waterline area, x_w the x coordinate of the center of the waterline, GM the metacentric height, GM_L the longitudinal metacentric height, and ω_g the circular natural frequency of yaw motions. ω_g is determined by the control characteristics of the autopilot and usually has little influence on the yaw motions in seaways. In computing GM_L, the moment of inertia is taken with respect to the origin of the coordinate system (usually amidships) and not, as usual, with respect to the center of the waterline. For corrections for dry transoms and unsymmetrical bodies reference is made to Söding (1987).

N is the damping matrix; it contains mainly the effect of the radiated waves. A is the added mass matrix. The decomposition of the force into hydrostatic (S) and hydrodynamic (A) components is somewhat arbitrary, especially for the ship with forward speed. Therefore, comparisons between computations and experiments are often based on the term $-\omega_e^2 A + S$.

$\overrightarrow{F}_e$ is the vector of exciting forces which a wave would exert on a ship fixed on its average position (diffraction problem). The exciting forces can be decomposed into a contribution due to the pressure distribution in the undisturbed incident wave (Froude−Krilov force) and the contribution due to the disturbance by the ship (diffraction force). Both contributions are of similar order of magnitude. To determine A and N, the flow due to the harmonic ship motions $\overrightarrow{u}$ must be computed (radiation problem). For small frequency of the motion (i.e. large wave length of the radiated waves), the hydrostatic forces dominate and the hydrodynamic forces are almost negligible. Therefore large relative errors in computing A and N are acceptable. For high

frequencies, the crests of the waves radiated by the ship motions are near the ship almost parallel to the ship hull, i.e. predominantly in the longitudinal direction. Therefore the longitudinal velocity component of the radiated waves can be neglected. Then only the two-dimensional flow around the ship sections (strips) must be determined. This simplifies the computations a great deal.

For the diffraction problem (disturbance of the wave due to the ship hull), which determines the exciting forces, a similar reasoning does not hold: unlike radiation waves (due to ship motions), diffraction waves (due to partial reflection at the hull and distortion beyond the hull) form a similar angle (except for sign) with the hull as the incident wave. Therefore, for most incident waves, the diffraction flow will also feature considerable velocities in the longitudinal direction. These cannot be considered in a regular strip method, i.e. if we want to consider all strips as hydrodynamically independent. This error is partially compensated by computing the diffraction flow for wave frequency ω instead of encounter frequency ω_e, but a residual error remains. To avoid these residual errors, sometimes $\overrightarrow{F}_e$ is determined indirectly from the radiation potential following formulae of Newman (1965). However, these formulae are only valid if the waterline is also streamline. This is especially not true for ships with submerged transom sterns.

For the determination of the radiation and (usually also) diffraction (= exciting) forces, the two-dimensional flow around an infinite cylinder of the same cross-section as the ship at the considered position is solved (Fig. 4.16). The flow is generated by harmonic motions of the cylinder (radiation) or an incident wave (diffraction). Classical methods used analytical solutions based on multipole methods. Today, usually two-dimensional panel methods are preferred due to their (slightly) higher accuracy for realistic ship geometries. These two-dimensional panel methods can be based on GFM or RSM (see Chapter 3).

The flow and thus the pressure distribution depend on:

- for the radiation problem: hull shape, frequency ω_e, and direction of the motion (vertical, horizontal, rotational)
- for the diffraction problem: hull shape, wave frequency ω, and encounter angle μ.

For the radiation problem, we compute the pressure distributions for unit amplitude motions in one degree of freedom and set all other motions to zero and omit the incident wave. For the diffraction problem, we set all motions to zero and consider only the incident wave and its diffraction. We denote the resulting pressures by:

$\widehat{p}_2$ for horizontal unit motion of the cylinder;
$\widehat{p}_3$ for vertical unit motion of the cylinder;
$\widehat{p}_4$ for rotational unit motion of the cylinder around the x axis;
$\widehat{p}_0$ for the fixed cylinder in waves (only the pressure in the undisturbed wave);
$\widehat{p}_7$ for the fixed cylinder in waves (only the disturbance of the pressure due to the body).

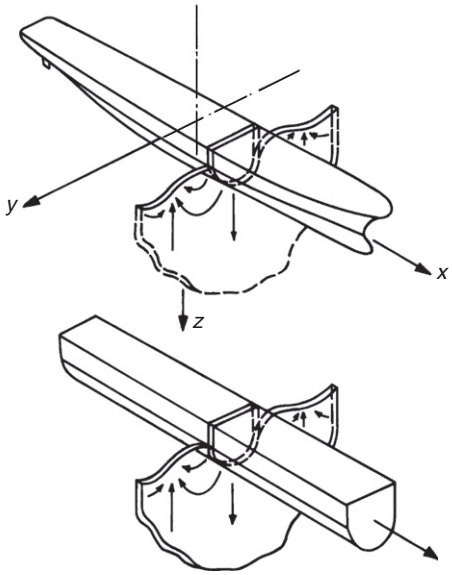

Figure 4.16:
Principle of strip method

Let the actual motions of the cylinder in a wave of amplitude $\widehat{h}_x$ be described by the complex amplitudes $\widehat{u}_{2,0x}$, $\widehat{u}_{3,0x}$, $\widehat{u}_{4,0x}$. Then the complex amplitude of the harmonic pressure is:

$$\widehat{p}_i = \widehat{p}_2\widehat{u}_{2,0x} + \widehat{p}_3\widehat{u}_{3,0x} + \widehat{p}_4\widehat{u}_{4,0x} + (\widehat{p}_0 + \widehat{p}_7)\widehat{h}_x \tag{4.52}$$

The amplitudes of the forces per length on the cylinder are obtained by integrating the pressure over the wetted surface of a cross-section (wetted circumference):

$$\begin{Bmatrix} \widehat{f}_2 \\ \widehat{f}_3 \\ \widehat{f}_4 \end{Bmatrix} = \int_0^l \begin{Bmatrix} n_2 \\ n_3 \\ yn_3 - zn_2 \end{Bmatrix} \cdot \widehat{p}_i \, \mathrm{d}\ell = \int_0^l \begin{Bmatrix} n_2 \\ n_3 \\ yn_3 - zn_2 \end{Bmatrix} \cdot \begin{Bmatrix} \widehat{p}_2 \\ \widehat{p}_3 \\ \widehat{p}_4 \\ \widehat{p}_0 + \widehat{p}_7 \end{Bmatrix}^T \mathrm{d}\ell \cdot \begin{Bmatrix} \widehat{u}_{2,0x} \\ \widehat{u}_{3,0x} \\ \widehat{u}_{4,0x} \\ \widehat{h}_x \end{Bmatrix} \tag{4.53}$$

$\{0, n_2, n_3\}$ is here in the inward unit normal on the cylinder surface. The index x in the last vector indicates that all quantities are taken at the longitudinal coordinate x at the ship, i.e. the position of the strip under consideration. ℓ is the circumferential length coordinate of the wetted contour. We can write the above equation in the form:

$$\overrightarrow{\widehat{f}} = \widehat{H} \cdot \left\{ \widehat{u}_{2,0x}, \widehat{u}_{3,0x}, \widehat{u}_{4,0x}, \widehat{h}_x \right\}^T \tag{4.54}$$

The elements of the matrix $\widehat{H}$, obtained by the integrals over the wetted surface in the above original equation, can be interpreted as added masses a_{ij}, damping n_{ij} and exciting forces per wave amplitude $\widehat{f}_{ei}$:

$$\widehat{H} = \begin{bmatrix} \omega_e^2 a_{22} - i\omega_e n_{22} & 0 & \omega_e^2 a_{24} - i\omega_e n_{24} & \widehat{f}_{e2} \\ 0 & \omega_e^2 a_{33} - i\omega_e n_{33} & 0 & \widehat{f}_{e3} \\ \omega_e^2 a_{42} - i\omega_e n_{42} & 0 & \omega_e^2 a_{44} - i\omega_e n_{44} & \widehat{f}_{e4} \end{bmatrix} \tag{4.55}$$

For example, a_{22} is the added mass per cylinder length for horizontal motion.

The added mass tends towards infinity as the frequency goes to zero. However, the effect of the added mass also goes to zero for small frequencies, as the added mass is multiplied by the square of the frequency.

The forces on the total ship are obtained by integrating the forces per length (obtained for the strips) over the ship length. For forward speed, the harmonic pressure according to the linearized Bernoulli equation also contains a product of the constant ship speed $-V$ and the harmonic velocity component in the x direction. Also, the strip motions denoted by index x have to be converted to global ship motions in six degrees of freedom. This results in the global equation of motion:

$$\left[S - \omega_e^2 (M + \widehat{B})\right] \widehat{u} = \widehat{E} h \tag{4.56}$$

$\widehat{B}$ is a complex matrix. Its real part is the added mass matrix A. Its imaginary part is the damping matrix N:

$$\omega_e^2 \widehat{B} = \omega_e^2 A - i\omega_e N = \int_L V(x) \cdot \left(1 + \frac{iV}{\omega_e} \frac{\partial}{\partial x}\right) \left(\widehat{H}_B \cdot W(x)\right) \mathrm{d}x \tag{4.57}$$

This equation can be used directly to compute $\widehat{B}$, e.g. using the trapezoidal rule for the integrals and numerical difference schemes for the differentiation in x. Alternatively, partial integration can remove the x derivatives. The new quantities in the above equations are defined as:

$$\widehat{\overrightarrow{E}} = \frac{\widehat{\overrightarrow{F}}_E}{h} = \int_L V(x) \cdot \left(\widehat{H}_E + \frac{iV}{\omega} \frac{\partial \widehat{H}_{E7}}{\partial x}\right) \mathrm{e}^{ikx\cos\mu} \, \mathrm{d}x \tag{4.58}$$

$$W(x) = \begin{bmatrix} 0 & 1 & 0 & t_x & 0 & x - V/(i\omega_e) \\ 0 & 0 & 1 & 0 & -x + V/(i\omega_e) & 0 \\ 0 & 0 & 0 & 1 & 0 & 0 \end{bmatrix} \tag{4.59}$$

t_x is the z coordinate (in the global ship system) of the origin of the reference system for a strip. (Often a strip reference system is chosen with origin in the waterline, while the global ship coordinate system may have its origin on the keel.)

$$V(x) = \begin{bmatrix} 1 & 0 & 0 & 0 & 0 \\ 0 & 1 & 0 & 0 & 0 \\ 0 & 0 & 1 & 0 & 0 \\ 0 & t_x & 0 & 1 & 0 \\ -t_x & 0 & -x & 0 & 1 \\ 0 & x & 0 & 0 & 0 \end{bmatrix} \tag{4.60}$$

$$\widehat{H}_B = \begin{bmatrix} 0 & 0 & 0 \\ \omega_e^2 a_{22} - i\omega_e n_{22} & 0 & \omega_e^2 a_{24} - i\omega_e n_{24} \\ 0 & \omega_e^2 a_{33} - i\omega_e n_{33} & 0 \\ \omega_e^2 a_{42} - i\omega_e n_{42} & 0 & \omega_e^2 a_{44} - i\omega_e n_{44} \\ 0 & 0 & 0 \end{bmatrix} \tag{4.61}$$

$$\widehat{H}_E = \begin{Bmatrix} -i\rho g k A_x \cos\mu \\ \widehat{f}_{e2} \\ \widehat{f}_{e3} \\ \widehat{f}_{e4} \\ -i\rho g k A_x s_x \cos\mu \end{Bmatrix} \tag{4.62}$$

A_x is the submerged section area at x; s_x is the vertical coordinate of the center of the submerged section area in the global system. $\widehat{H}_E$ contains both the Froude−Krilov part from the undisturbed wave (Index 0) and the diffraction part (Index 7), while $\widehat{H}_{E7}$ contains only the diffraction part.

The formulae for $\widehat{B}$ and $\widehat{\overrightarrow{E}}$ contain x derivatives. At locations x, where the ship cross-section changes suddenly (propeller aperture, vertical stem, submerged transom stern), this would result in extremely high forces per length. To a large extent, this is actually true at the bow, but not at the stern. If the cross-sections decrease rapidly there, the streamlines separate from the ship hull. The momentum (which equals added mass of the cross-section times velocity of the cross-section) then remains in the ship's wake while the above formulae would yield in strict application zero momentum behind the ship as the added mass is zero there. Therefore, the integration of the x derivatives over the ship length in the above formulae has to end at such locations of flow separation in the aftbody.

The global equation of motion above yields the vector of the response amplitude operators (RAOs) (= complex amplitude of reaction/wave amplitude) for the ship motions:

$$\frac{\widehat{u}}{h} = \left(S - \omega_e^2[M + \widehat{B}]\right)^{-1} \cdot \widehat{\overrightarrow{E}} \tag{4.63}$$

The effect of rudder actions due to course deviations (yaw oscillations) was already considered in the matrix S. In addition, there are forces on the rudder (and thus the ship) due to ship motions (for centrally located rudders only due to sway, yaw, and roll) and due to the incident wave. Here it is customary to incorporate the rudder in the model of the rigid ship filling the gaps between rudder and ship. (While this is sufficient for the computation of the ship motions, it is far too crude if the forces on the rudder in a seaway are to be computed.)

Accurate computation of the motions, pressures, internal forces, etc. requires further additions and corrections, e.g. to capture the influence of non-linear effects especially for roll motion, treatment of low encounter frequencies, influence of bilge keels, stabilizing fins, etc. The special and often empirical treatment of these effects differs in various strip methods. Details can be found in the relevant specialized literature.

4.4.3. Rankine Singularity Methods

Bertram and Yasukawa (1996) give an extensive survey of these methods. A linear frequency-domain method is described briefly here to exemplify the general approach.

In principle, RSM can consider the steady potential completely. If ϕ^s is completely captured the methods are called 'fully three-dimensional' to indicate that they capture both the steady and the harmonic flow three-dimensionally. In this case, first the 'fully non-linear' wave resistance problem is solved to determine ϕ^s and its derivatives, including second derivatives of ϕ^s on the hull. The solution also yields all other steady flow effects, namely dynamic trim and sinkage, steady wave profile on the hull, and the steady wave pattern on the free surface. Then the actual seakeeping computations can be performed considering the interaction between steady and harmonic flow components. The boundary conditions for ϕ^I are linearized with regard to wave amplitude h and quantities proportional to h, e.g. ship motions. The Laplace equation (mass conservation) is solved subject to the boundary conditions:

1. Water does not penetrate the hull.
2. Water does not penetrate the free surface.
3. At the free surface there is atmospheric pressure.
4. Far away from the ship, the flow is undisturbed.
5. Waves generated by the ship radiate away from the ship.

6. Waves generated by the ship are not reflected at the artificial boundary of the computational domain.
7. For antisymmetric motions (sway, roll, yaw), a Kutta condition is enforced on the stern.
8. Forces (and moments) not in equilibrium result in ship motions.

For $\tau = \omega_e V/g > 0.25$ waves generated by the ship travel only downstream, similar to the steady wave pattern. Thus also the same numerical techniques as for the steady wave resistance problem can be used to enforce proper radiation, e.g. shifting source elements relative to collocation points downstream. Values $\tau < 0.25$ appear especially in following waves. Various techniques have been proposed for this case, as discussed in Bertram and Yasukawa (1996). However, there is no easy and accurate way in the frequency domain. In the time domain, proper radiation follows automatically and numerical beaches have to be introduced to avoid reflection at the outer boundary of the computational domain.

We split here the six-component motion vector of the section on the strip method approach into two three-component vectors. $\overrightarrow{u} = \{u_1, u_2, u_3\}^T$ describes the translations, $\overrightarrow{\alpha} = \{\alpha_1, \alpha_2, \alpha_3\}^T$ the rotations. The velocity potential is again decomposed as in Section 4.4.1:

$$\phi^t = (-Vx + \phi^s) + (\phi^w + \phi^I) \tag{4.64}$$

The steady potential ϕ^s is determined first. Typically, a 'fully non-linear' wave resistance code employing higher-order panels is also used to determine second derivatives of the potential on the hull. Such higher-order panels are described in the section on boundary elements. ϕ^w is the incident wave as in Section 4.3:

$$\phi^w = \mathrm{Re}(-ic\widehat{h}\mathrm{e}^{-kz}\mathrm{e}^{-ik(x\cos\mu - y\sin\mu)}\mathrm{e}^{i\omega_e t}) \tag{4.65}$$

The wave amplitude is chosen to $\widehat{h} = 1$. The remaining unknown potential ϕ^I is decomposed into diffraction and radiation components:

$$\phi^I = \phi^d + \sum_{i=1}^{6} \phi^i u_i \tag{4.66}$$

The boundary conditions 1−3 and 7 are numerically enforced in a collocation scheme, i.e. at selected individual points. The remaining boundary conditions are automatically fulfilled in a Rankine singularity method. Combining 2 and 3 yields the boundary condition on the free surface, to be fulfilled by the unsteady potential $\phi^w + \phi^I$:

$$\left(-\omega_e^2 + Bi\omega_e\right)\widehat{\phi}^{(1)} + \left(\left[2i\omega_e + B\right]\nabla\phi^{(0)} + \overrightarrow{a}^{(0)} + \overrightarrow{a}^{g}\right)\nabla\widehat{\phi}^{(1)} + \nabla\phi^{(0)}(\nabla\phi^{(0)}\nabla)\nabla\widehat{\phi}^{(1)} = 0 \tag{4.67}$$

with:

$$\phi^{(0)} = -Vx + \phi^s \quad \text{steady potential} \tag{4.68}$$

$$\vec{a}^{(0)} = (\nabla\phi^{(0)}\nabla)\nabla\phi^{(0)} \quad \text{steady particle acceleration} \tag{4.69}$$

$$\vec{a}^{g} = \vec{a} - \{0, 0, g\}^T \tag{4.70}$$

$$B = -\frac{1}{a_3^g}\,\frac{\partial(\nabla\phi^{(0)}\vec{a}^{g})}{\partial z} \tag{4.71}$$

$$\nabla = \{\partial/\partial x, \partial/\partial y, \partial/\partial z\}^T \tag{4.72}$$

The boundary condition 1 yields on the ship hull:

$$\vec{n}\nabla\widehat{\phi}^{(1)} + \widehat{\vec{u}}(\vec{m} - i\omega_e\vec{n}) + \widehat{\vec{\alpha}}[\vec{x} \times (\vec{m} - i\omega_e\vec{n}) + \vec{n} \times \nabla\phi^{(0)}] = 0 \tag{4.73}$$

Here the m-terms have been introduced:

$$\vec{m} = (\vec{n}\nabla)\nabla\phi^{(0)} \tag{4.74}$$

Vectors $\vec{n}$ and $\vec{x}$ are to be taken in the ship-fixed system.

The diffraction potential ϕ^d and the six radiation potentials ϕ^i are determined in a panel method that can employ regular first-order panels. The panels are distributed on the hull and on (or above) the free surface around the ship. The Kutta condition requires the introduction of additional dipole (or alternatively vortex) elements.

Test computations for a container ship (standard ITTC test case S-175) have shown a significant influence of the Kutta condition for sway, yaw, and roll motions for small encounter frequencies.

To determine ϕ^d, all motions (u_i, $i = 1$ to 6) are set to zero. To determine the ϕ^i, the corresponding u_i is set to 1, all other motion amplitudes, ϕ^d and ϕ^w to zero. Then the boundary conditions form a system of linear equations for the unknown element strengths which is solved, for example, by Gauss elimination. Once the element strengths are known, all potentials and derivatives can be computed.

For the computation of the total potential ϕ^t, the motion amplitudes u_i remain to be determined. The necessary equations are supplied by the momentum equations:

$$m(\ddot{\vec{u}} + \ddot{\vec{\alpha}} \times \vec{x}_g) = -\vec{\alpha} \times \vec{G} + \int (p^{(1)} - \rho[\vec{u}\vec{a}^{g} + \vec{\alpha}(\vec{x} \times \vec{a}^{g})]\vec{n}\,\mathrm{d}S \tag{4.75}$$

$$\begin{aligned} m(\vec{x}_g \times \ddot{\vec{u}}) + I\ddot{\vec{\alpha}} = -\vec{x}_g \times (\vec{\alpha} \times \vec{G}) + \int (p^{(1)} - \rho[\vec{u}\vec{a}^{g} + \vec{\alpha}(\vec{x} \times \vec{a}^{g})] \\ \times(\vec{x} \times \vec{n})\,\mathrm{d}S \end{aligned} \tag{4.76}$$

$G = gm$ is the ship's weight, $\vec{x}_g$ its center of gravity and I the matrix of the moments of inertia of the ship (without added masses) with respect to the coordinate system. I is the lower-right 3×3 sub-matrix of the 6×6 matrix M given in the section for the strip method.

The integrals extend over the average wetted surface of the ship. The harmonic pressure $p^{(1)}$ can be decomposed into parts due to the incident wave, due to diffraction, and due to radiation:

$$p^{(1)} = p^w + p^d + \sum_{i=1}^{6} p^i u_i \tag{4.77}$$

The pressures p^w, p^d and p^i, collectively denoted by p^j, are determined from the linearized Bernoulli equation as:

$$p^j = -\rho(\phi_t^j + \nabla\phi^{(0)}\nabla\phi^j) \tag{4.78}$$

The two momentum vector equations above form a linear system of equations for the six motions, u_i, which is easily solved.

The explicit consideration of the steady potential s changes the results for computed heave and pitch motions for wavelengths of similar magnitude as the ship length − these are the wavelengths of predominant interest − by as much as 20−30% compared to total neglect. The results for standard test cases such as the Series-60 and the S-175 agree much better with experimental data for the 'fully three-dimensional' method. For the standard ITTC test case of the S-175 container ship, in most cases good agreement with experiments could be obtained (Fig. 4.17). Only for low encounter frequencies are the antisymmetric motions over-predicted, probably because viscous effects and autopilot were not modeled at all in the computations.

If the steady flow is approximated by double-body flow, similar results are obtained as long as the dynamic trim and sinkage are small. However, the computational effort is nearly the same.

Japanese experiments on a tanker model indicate that for full hulls the diffraction pressures in the forebody for short head waves ($\lambda/L = 0.3$ and 0.5) are predicted with errors of up to 50% if ϕ^s is neglected (as typically in GFM or strip methods). Computations with and without consideration of ϕ^s yield large differences in the pressures in the bow region for radiation in short waves and for diffraction in long waves.

4.4.4. Problems for Fast and Unconventional Ships

Seakeeping computations are problematic for fast and unconventional ships. Seakeeping plays a special role here, as fast ships are often passenger ferries, which need good seakeeping characteristics to attract passengers. This is the reason why, for instance, planing boats with their bad seakeeping are hardly ever used for commercial passenger transport. For fast cargo ships, the reduced speed in seaways can considerably influence transport

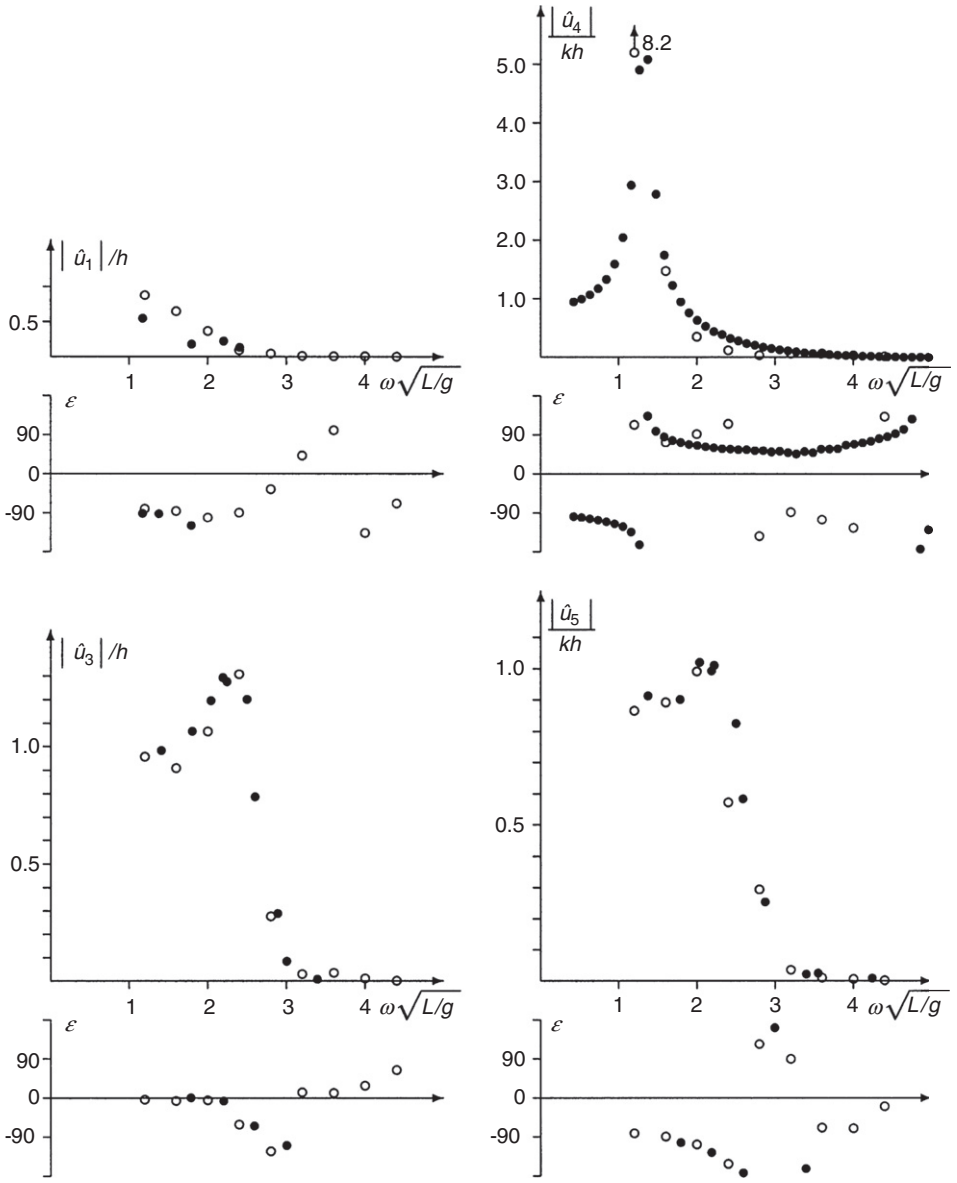

Figure 4.17:
Selected response amplitude operators of motions for the container ship S-175 at $F_n = 0.275$: experiment, computation surge (top left) for $\mu = 180°$; roll (top right) for $\mu = 120°$; heave (bottom left) for $\mu = 150°$; pitch (bottom right) for $\mu = 150°$

efficiency. A hull form, which is superior in calm water, may well become inferior in moderate seaways. Warships also often require good seakeeping to supply stable platforms for weapon systems, helicopters, or planes.

Unfortunately, computational methods for conventional ships are usually not at all or only with special modifications suitable for fast and unconventional ships. The special 'high-speed strip theory' (see Section 4.4.1) has been successfully applied in various forms to both fast monohulls and multihulls. Japanese validation studies showed that for a fast monohull with transom stern the HSST fared much better than both conventional strip methods and three-dimensional GFM and RSM. However, the conventional strip methods and the three-dimensional methods did not use any special treatment of the large transom stern of the test case. This impairs the validity of the conclusions. Researchers at the MIT have shown that at least for time-domain RSM the treatment of transom sterns is possible and also yields good results for fast ships, albeit at a much higher computational effort than the HSST. In most cases, HSST should yield the best cost–benefit ratio for fast ships.

It is often claimed in the literature that conventional strip methods are only suitable for low ship speeds. However, benchmark tests show that strip methods can yield good predictions of motion RAOs up to Froude numbers $F_n \approx 0.6$, provided that proper care is taken and the dynamic trim and sinkage and the steady wave profile at the hull are included to define the average submergence of the strips. The prediction of dynamic trim and sinkage is relatively easy for fast displacement ships, but difficult for planing boats. Neglecting these effects, i.e. computing for the calm-water wetted surface, may be a significant reason why often a lower Froude number limit of $F_n \approx 0.4$ is cited in the literature.

For catamarans, the interaction between the hulls plays an important role especially for low speeds. For design speed, the interaction is usually negligible in head seas. Three-dimensional methods (RSM, GFM) capture automatically the interaction as both hulls are simultaneously modeled. The very slender form of the demihulls introduces smaller errors for GFM catamaran computations than for monohulls. Both RSM and GFM applications to catamarans can be found in the literature, usually for simplified research geometries. Strip methods require special modifications to capture, at least in good approximation, the hull interaction, namely multiple reflection of radiation and diffraction waves. Simply using the hydrodynamic coefficients for the two-dimensional flow between the two cross-sections leads to strong overestimation of the interaction for $V > 0$.

Seakeeping computations for air-cushioned vehicles and surface effect ships are particularly difficult due to additional problems:

- The flexible skirts deform under the changing air cushion pressure and the contact with the free surface. Thus the effective cushion area and its center of gravity change.
- The flow and the pressure in the cushion contain unsteady parts which depend strongly on the average gap between free surface and skirts.
- The dynamics of fans (and their motors) influences the ship motions.

In particular the narrow gaps between skirts and free surface result in a strongly non-linear behavior that so far excludes accurate predictions.

4.4.5. Further Quantities in Regular Waves

Within a linear theory, the velocity and acceleration RAOs can be directly derived, once the motion RAOs are determined. The relative motion between a point on the ship and the water surface is important to evaluate the danger of slamming or water on deck. The RAOs for relative motion should incorporate the effect of diffraction and radiation, which is again quite simple once the RAOs for the ship motions are determined. However, effects of flared hull shape with outward forming spray for heave motion cannot be modeled properly within a linear theory, because these depend non-linearly on the relative motion. In practice, the section flare is important for estimating the amount of water on deck.

Internal forces on the ship hull (longitudinal, transverse, and vertical forces, torsional, transverse, and longitudinal bending moments) can also be determined relatively easily for known motions. The pressures are then only integrated up to a given cross-section instead of over the whole ship length. (Within a strip method approach, this also includes the matrix of restoring forces S, which contains implicitly many hydrostatic pressure terms.) Also, the mass forces (in matrix M) should only be considered up to the given location x of the cross-section. Stresses in the hull can then be derived from the internal forces. However, care must be taken that the moments are transformed to the neutral axis of the 'beam' ship hull. Also, stresses in the hull are often of interest for extreme loads where linear theory should no longer be applied.

The longitudinal force on the ship in a seaway is to first order within a linear theory also a harmonically oscillating quantity. The time average of this quantity is zero. However, in practice the ship experiences a significantly non-zero added resistance in seaways. This added resistance (and similarly the transverse drift force) can be estimated using linear theory. Two main contributions appear:

- Second-order pressure contributions are integrated over the average wetted surface.
- First-order pressure contributions are integrated over the difference between average and instantaneous wetted surface; this yields an integral over the contour of the waterplane.

If the steady flow contribution is completely retained (as in some three-dimensional BEM), the resulting expression for the added resistance is rather complicated and also involves second derivatives of the potential on the hull. Usually this formula is simplified assuming:

- uniform flow as the steady base flow;
- dropping a term involving x-derivatives of the flow;
- considering only heave and pitch as main contributions to added resistance.

4.4.6. Ship Responses in Stationary Seaway

Here the issue is how to get statistically significant properties in natural seaways from a response amplitude operator $Y_r(\omega,\mu)$ in elementary waves for an arbitrary response r depending linearly on wave amplitude. The seaway is assumed to be stationary with known spectrum $S_\zeta(\omega,\mu)$.

Since the spectrum is a representation of the distribution of the amplitude squared over ω and μ, and the RAO $\widehat{Y}_r$ is the complex ratio of r_A/ζ_A, the spectrum of r is given by:

$$S_r(\omega,\mu) = |Y_r(\omega,\mu)|^2 S_\zeta(\omega,\mu) \tag{4.79}$$

Values of r, chosen at a random point in time, follow a Gaussian distribution. The average of r is zero if we assume $r \sim \zeta_A$, i.e. in calm water $r = 0$. The probability density of randomly chosen r values is:

$$f(r) = \frac{1}{\sqrt{2\pi}\sigma_r} \exp\left(-\frac{r^2}{2\sigma_r^2} \right) \tag{4.80}$$

The variance σ_r^2 is obtained by adding the variances due to the elementary waves in which the natural seaway is decomposed:

$$\sigma_r^2 = \int_0^\infty \int_0^{2\pi} S_r(\omega,\mu)\, \mathrm{d}\mu\, \mathrm{d}\omega \tag{4.81}$$

The sum distribution corresponding to the frequency density $f(r)$ above is:

$$F(r) = \int_{-\infty}^{r} f(\rho)\ \mathrm{d}\rho = \frac{1}{2}[1 + \phi(r/\sigma_r)] \tag{4.82}$$

The probability integral ϕ is defined as:

$$\phi = \frac{2}{\sqrt{2\pi}} \int_{-\infty}^{x} \mathrm{e}^{-t^2/2}\, \mathrm{d}t \tag{4.83}$$

$F(r)$ gives the percentage of time when a response (in the long-term average) is less or equal to a given limit r. $1 - F(r)$ is then the corresponding percentage of time when the limit r is exceeded.

More often the distribution of the amplitudes of r is of interest. We define here the amplitude of r (differing from some authors) as the maximum of r between two following upward zero

crossings (where $r = 0$ and $\dot{r} > 0$). The amplitudes of r are denoted by r_A. They have approximately (except for extremely 'broad' spectra) the following probability density:

$$f(r_A) = \frac{r_A}{\sigma_r^2} \exp\left(-\frac{r_A^2}{2\sigma_r^2}\right) \tag{4.84}$$

The corresponding sum distribution is:

$$F(r_A) = 1 - \exp\left(-\frac{r_A^2}{2\sigma_r^2}\right) \tag{4.85}$$

σ_r follows again from Eq. (4.81). The formula for $F(r_A)$ describes a so-called Rayleigh distribution. The probability that a randomly chosen amplitude of the response r exceeds r_A is:

$$1 - F(r_A) = \exp\left(-\frac{r_A^2}{2\sigma_r^2}\right) \tag{4.86}$$

The average frequency (occurrences/time) of upward zero crossings is derived from the r spectrum to:

$$f_0 = \frac{1}{2\pi\sigma_r} \sqrt{\int_0^\infty \int_0^{2\pi} \omega_e^2 S_r(\omega, \mu)\, \mathrm{d}\mu\, \mathrm{d}\omega} \tag{4.87}$$

Together with Eq. (4.86) this yields the average occurrence of r amplitudes which exceed a limit r_A during a period T:

$$z(r_A) = T f_0 \exp\left(-\frac{r_A^2}{2\sigma_r^2}\right) \tag{4.88}$$

Often we are interested in questions such as, 'What is the probability that during a period T a certain stress is exceeded in a structure or an opening is flooded?' Generally, the issue is then the probability $P_0(r_A)$ that during a period T the limit r_A is never exceeded. In other words, $P_0(r_A)$ is the probability that the maximum amplitude during the period T is less than r_A. This is given by the sum function of the distribution of the maximum of r during T. We make two assumptions:

- $z(r_A) << T f_0$; this is sufficiently well fulfilled for $r_A \geq 2\sigma_r$.
- An amplitude r_A is statistically nearly independent of its predecessors. This is true for most seakeeping responses, but not for the weakly damped amplitudes of elastic ship vibration excited by seaway, for example.

Under these assumptions we have:

$$P_0(r_A) = \mathrm{e}^{-z(r_A)} \tag{4.89}$$

If we insert here the above expression for $z(r_A)$ we obtain the 'double' exponential distribution typical for the distribution of extreme values:

$$P_0(r_A) = \mathrm{e}^{-Tf_0 \exp(-r_A^2/(2\sigma_r^2))} \tag{4.90}$$

The probability of exceedence is then $1 - P_0(r_A)$. Under the (far more limiting) assumption that $z(r_A) << 1$ we obtain the approximation:

$$1 - P_0(r_A) \approx z(r_A) \tag{4.91}$$

The equations for $P_0(r_A)$ assume neither a linear correlation of the response r from the wave amplitude nor a stationary seaway. They can therefore also be applied to results of non-linear simulations or long-term distributions.

4.4.7. Time-Domain Simulation Methods

The appropriate tools to investigate strongly non-linear ship reactions are simulations in the time domain. The seaway itself is usually linearized, i.e. computed as superposition of elementary waves. The frequencies of the individual elementary waves ω_j may not be integer multiples of a minimum frequency $\omega_{\min}$. In this case, the seaway would repeat itself after $2\pi/\omega_{\min}$ unlike a real natural seaway. Appropriate methods to choose the ω_j are:

- The ω_j are chosen such that the area under the sea spectrum between ω_j and ω_{j+1} is the same for all j. This results in constant amplitudes for all elementary waves regardless of frequency.
- The frequency interval of interest for the simulation is divided into intervals. These intervals are larger where S_ζ or the important RAOs are small and vice versa. In each interval a frequency ω_j is chosen randomly (based on constant probability distribution). One should not choose the same ω_j for all the L encounter angles under consideration. Rather each combination of frequency ω_j and encounter angle μ_l should be chosen anew and randomly.

The frequencies, encounter angles, and phase angles chosen before the simulation must be kept during the whole simulation.

Starting from a realistically chosen start position and velocity of the ship, the simulation computes in each time step the forces and moments acting from the moving water on the ship. The momentum equations for translations and rotations give the translational and rotational accelerations. Both are three-component vectors and are suitably expressed in a ship-fixed coordinate system. The momentum equations form a system of six scalar, coupled ordinary second-order differential equations. These can be transformed into a system of 12 first-order differential equations which can be solved by standard methods, e.g. fourth-order Runge−Kutta integration. This means that the ship position and velocity at the end of a small

time interval, e.g. 1 second, are determined from the corresponding data at the beginning of this interval using the computed accelerations.

The forces and moments can be obtained by integrating the pressure distribution over the momentary wetted ship surface. Three-dimensional methods are usually too expensive for this purpose. Therefore modified strip methods are most frequently used. A problem is that the pressure distribution depends not only on the momentary position, velocity, and acceleration, but also on the history of the motion which is reflected in the wave pattern. This effect is especially strong for heave and pitch motions. In computations for the frequency domain, the historical effect is expressed in the frequency dependency of the added mass and damping. In time-domain simulations, we cannot consider a frequency dependency because there are many frequencies at the same time and the superposition principle does not hold. Therefore, the historical effect on the hydrodynamic forces and moments $\vec{F}$ is either expressed in convolution integrals ($\vec{u}$ contains here not only the ship motions, but also the incident waves):

$$\vec{F}(t) = \int_{-\infty}^{t} K(\tau)\,\vec{u}(\tau)\,\mathrm{d}\tau \tag{4.92}$$

Or one considers 0 to n time derivatives of the forces $\vec{F}$ and 1 to $(n+1)$ time derivatives of the motions $\vec{u}$:

$$B_0\vec{F}(t) + B_1\dot{\vec{F}}(t) + B_2\ddot{\vec{F}}(t) + \ldots = A_0\dot{\vec{u}}(t) + A_1\ddot{\vec{u}}(t) + A_0\dddot{\vec{u}}(t) + \ldots \tag{4.93}$$

The matrix $K(\tau)$ in the first alternative and the scalars A_i, B_i in the second alternative are determined in potential flow computations for various sinkage and heel of the individual strips.

The second alternative is called the state model and appears to be far superior to the first alternative. Typical values for n are 2−4; for larger n, problems occur in the determination of the constants A_i and B_i resulting, for example, in numerically triggered oscillations. Pereira (1988) gives details of such a simulation method, namely SIMBEL. The simulation method has been extended considerably in the meantime and can also consider simultaneously the flow of water through a damaged hull, sloshing of water in the hull, or water on deck.

A far simpler and far faster approach is described, e.g., in Söding (1987). Here only the strongly non-linear surge and roll motions are determined by a direct solution of the equations of motion in the time-domain simulation (code ROLLS). The other four degrees of freedom are linearized and then treated similarly as the incident waves, i.e. they are computed from RAOs in the time domain. This is necessary to couple the four linear motions to the two non-linear motions. (Roll motions are often simulated as independent from the other motions, but this yields totally unrealistic results.) The restriction to surge and roll much simplifies the computation, because the history effect for these degrees of freedom is negligible. Extensive validation studies for this approach with model tests gave excellent agreement for capsizing of

damaged ro-ro vessels drifting without forward speed in transverse waves (Chang and Blume 1998).

Simulations often aim to predict the average occurrence $z(r_A)$ of incidents where in a given period T a seakeeping response $r(t)$ exceeds a limit r_A. A new incident is then counted when after a previous incident another zero crossing of r occurred. The average occurrence is computed by multiple simulations with the characteristic data, but other random phases ε_{jl} for the superposition of the seaway. Alternatively, the simulation time can be chosen as nT and the number of occurrences can be divided by n. Both alternatives yield the same results except for random fluctuations.

Often seldom (extremely unlikely) incidents are of interest which would require simulation times of weeks to years to determine $z(r_A)$ directly if the occurrences are determined as described above. However, these incidents are expected predominantly in the presence of one or several particularly high waves. One can then reduce the required simulation time drastically by substituting the real seaway of significant wave height H_{real} by a seaway with larger significant wave height H_{sim}. The periods of both seaways shall be the same. The following relation between the incidents in the real seaway and in the simulated seaway exists (Söding 1987):

$$\frac{H_{\text{sim}}^2}{H_{\text{real}}^2} = \frac{\ln[z_{\text{real}}(r_A)/z(0)] + 1.25}{\ln[z_{\text{sim}}(r_A)/z(0)] + 1.25} \tag{4.94}$$

This equation is sufficiently accurate for $z_{\text{sim}}/z(0) < 0.03$. In practice, one determines in simulated seaway, e.g. with 1.5−2 times larger significant wave height, the occurrences $z_{\text{sim}}(r_A)$ and $z(0)$ by direct counting; then Eq. (4.94) is solved for the unknown $z_{\text{real}}(r_A)$:

$$z_{\text{real}}(r_A) = z(0)\exp\left(\frac{H_{\text{sim}}^2}{H_{\text{real}}^2}\{\ln[z_{\text{sim}}(r_A)/z(0)] + 1.25\} - 1.25\right) \tag{4.95}$$

4.4.8. Long-Term Distributions

Section 4.4.6 treated ship reactions in stationary seaway. This section will cover probability distributions of ship reactions r during periods T with changing sea spectra. A typical example for T is the total operational time of a ship. A quantity of interest is the average occurrence $z_L(r_A)$ of cases when the reaction $r(t)$ exceeds the limit r_A. The average can be thought of as the average over many hypothetical realizations, e.g. many equivalently operated sister ships.

First, one determines the occurrence $z(r_A;H_{1/3},T_p,\mu_0)$ of exceeding the limit in a stationary seaway with characteristics $H_{1/3}$, T_p, and μ_0 during total time T. (See Section 4.4.6 for linear

ship reactions and Section 4.4.7 for non-linear ship reactions.) The weighted average of the occurrences in various seaways is formed. The weighing factor is the probability $p(H_{1/3},T_p,\mu_0)$ that the ship encounters the specific seaway:

$$z_L(r_A) = \sum_{\text{all } H_{1/3}} \sum_{\text{all } T_p} \sum_{\text{all } \mu_0} z(r_A; H_{1/3}, T_p, \mu_0) \cdot p(H_{1/3}, T_p, \mu_0) \tag{4.96}$$

Usually, for simplification, it is assumed that the ship encounters seaways with the same probability under n_μ encounter angles μ_0:

$$z_L(r_A) = \frac{1}{n_\mu} \sum_{\text{all } H_{1/3}} \sum_{\text{all } T_p} \sum_{i=1}^{n_\mu} z(r_A; H_{1/3}, T_p, \mu_{0i}) \cdot p(H_{1/3}, T_p) \tag{4.97}$$

The probability $p(H_{1/3},T_p)$ for encountering a specific seaway can be estimated using data as given in Table 4.2. If the ship were to operate exclusively in the ocean area for Table 4.2, the table values (divided by 10^6) could be taken directly. This is not the case in practice and requires corrections. A customary correction then is to base the calculation only on 1/50 or 1/100 of the actual operating time of the ship. This correction considers, e.g.:

- The ship usually operates in areas with not quite so strong seaways as given in Table 4.2.
- The ship tries to avoid particularly strong seaways.
- The ship reduces speed or changes course relative to the dominant wave direction, if it cannot avoid a particularly strong seaway.
- Some exceedence of r_A is not important, e.g. for bending moments if they occur in load conditions when the ship has only a small calm-water bending moment.

The sum distribution of the amplitudes r_A, i.e. the probability that an amplitude r is less than a limit r_A, follows from z_L:

$$P_L(r_A) = 1 - \frac{z_L(r_A)}{z_L(0)} \tag{4.98}$$

$z_L(0)$ is the number of amplitudes during the considered period T. This distribution is used for seakeeping loads in fatigue strength analyses of the ship structure. It is often only slightly different from an exponential distribution, i.e. it has approximately the sum distribution:

$$P_L(r_A) = 1 - \mathrm{e}^{-r_A/r_0} \tag{4.99}$$

r_0 is a constant describing the load intensity. (In fatigue strength analyses, often the logarithm of the exceedence probability $\log(1 - P_L)$ is plotted over r_A; since for an exponential distribution the logarithm results in a straight line, this is called a log-linear distribution.)

The probability distribution of the largest loads during the period T can be determined from (see Section 4.4.6 for the underlying assumptions):

$$P_0(r_A) = \mathrm{e}^{-z(r_A)} \tag{4.100}$$

The long-term occurrence $z_L(r_A)$ of exceeding the limit r_A is inserted here for $z(r_A)$.

4.5. Slamming

In rough seas with large relative ship motion, slamming may occur with large water impact loads. Usually, slamming loads are much larger than other wave loads. Sometimes ships suffer local damage from the impact load or large-scale buckling on the deck. For high-speed ships, even if each impact load is small, frequent impact loads accelerate fatigue failures of hulls. Thus, slamming loads may threaten the safety of ships. The expansion of ship size and new concepts in fast ships have decreased relative rigidity, causing in some cases serious wrecks.

A rational and practical estimation method of wave impact loads is one of the most important prerequisites for safety design of ships and ocean structures. Wave impact has challenged many researchers since von Karman's work in 1929. Today, mechanisms of wave impacts are correctly understood for the two-dimensional case, and accurate impact load estimation is possible for the deterministic case. The long-term prediction of wave impact loads can also be given in the framework of linear stochastic theories. However, our knowledge on wave impact is still insufficient. A fully satisfactory theoretical treatment has been prevented so far by the complexity of the problem:

- Slamming is a strongly non-linear phenomenon, which is very sensitive to relative motion and contact angle between body and free surface.
- Predictions in natural seaways are inherently stochastic; slamming is a random process in reality.
- Since the duration of wave impact loads is very short, hydro-elastic effects are large.
- Air trapping may lead to compressible, partially supersonic flows where the flow in the water interacts with the flow in the air.

Most theories and numerical applications are for two-dimensional rigid bodies (infinite cylinders or bodies of rotational symmetry), but slamming in reality is a strongly three-dimensional phenomenon. We will here briefly review the most relevant theories. Further recommended literature includes:

- Tanizawa and Bertram (1998) for practical recommendations translated from the Kansai Society of Naval Architects, Japan.
- Mizoguchi and Tanizawa (1996) for stochastic slamming theories.

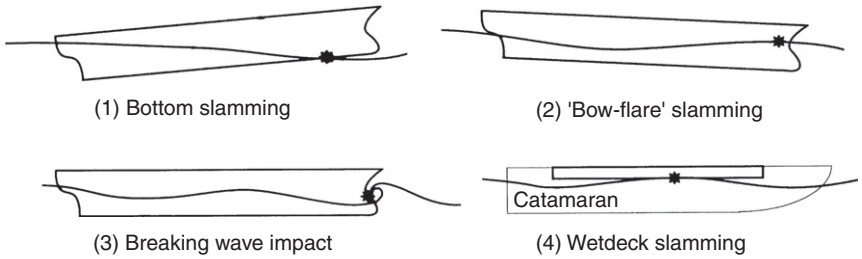

Figure 4.18:
Types of slamming impact of a ship

- Korobkin (1996) for theories with strong mathematical focus.
- SSC (1995) for a comprehensive compilation (more than 1000 references) of older slamming literature.

The wave impact caused by slamming can be roughly classified into four types (Fig. 4.18):

1. Bottom slamming occurs when emerged bottoms re-enter the water surface.
2. Bow-flare slamming occurs for high relative speed of bow-flare to the water surface.
3. Breaking wave impacts are generated by the superposition of incident wave and bow wave hitting the bow of a blunt ship even for small ship motion.
4. Wet-deck slamming occurs when the relative heaving amplitude is larger than the height of a catamaran's wet-deck.

Both bottom and bow-flare slamming occur typically in head seas with large pitching and heaving motions. All four water impacts are three-dimensional phenomena, but have been treated as two-dimensional for simplicity. For example, types 1 and 2 were idealized as two-dimensional wedge entry to the calm-water surface. Type 3 was also studied as a two-dimensional phenomenon similar to wave impact on breakwaters. We will therefore review two-dimensional theories first.

- *Linear slamming theories based on expanding thin-plate approximation*
  Classical theories approximate the fluid as inviscid, irrotational, incompressible, and free of surface tension. In addition, it is assumed that gravity effects are negligible. This allows a (predominantly) analytical treatment of the problem in the framework of potential theory.

  For bodies with small deadrise angle, the problem can be linearized. Von Karman (1929) was the first to study theoretically water impact (slamming). He idealized the impact as a two-dimensional wedge entry problem on the calm-water surface to estimate the water impact load on a seaplane during landing (Fig. 4.19). Mass, deadrise angle, and initial penetrating velocity of the wedge are denoted as m, β and V_0. Since the impact is so rapid, von Karman assumed very small water surface elevation during impact and negligible gravity effects. Then the added mass is approximately $m_v = 1/2\pi\rho c^2$. ρ is the water

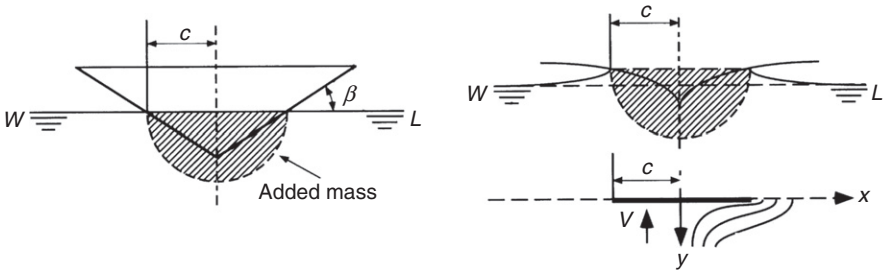

Figure 4.19:
Water impact models of von Karman (left) and Wagner (right)

density and c the half width of the wet area implicitly computed from $\mathrm{d}c/\mathrm{d}t = \cot\beta$. The momentum before the impact mV_0 must be equal to the sum of the wedge momentum mV and added mass momentum $m_v V$, yielding the impact load as:

$$P = \frac{V_0^2/\tan\beta}{\left(1+\dfrac{\rho\pi c^2}{2m}\right)^3}\cdot\rho\pi c \tag{4.101}$$

Since von Karman's impact model is based on momentum conservation, it is usually referred to as momentum impact, and because it neglects the water surface elevation, the added mass and impact load are underestimated, particularly for small deadrise angle. Wagner derived a more realistic water impact theory in 1932. Although he assumed still small deadrise angles in his derivation, the theory was found to be unsuitable for $\beta < 3°$, since then air trapping and compressibility of water play an increasingly important role. If β is assumed small and gravity neglected, the flow under the wedge can be approximated by the flow around an expanding flat plate in uniform flow with velocity V (Fig. 4.19). Using this model, the velocity potential and its derivative with respect to y on the plate $y = 0^+$ is analytically given as:

$$\phi = \begin{cases} V\sqrt{c^2-x^2} & \text{for } x < c \\ 0 & \text{for } x > c \end{cases} \tag{4.102}$$

$$\frac{\partial\phi}{\partial y} = \begin{cases} 0 & \text{for } x < c \\ V/\sqrt{1-c^2/x^2} & \text{for } x > c \end{cases} \tag{4.103}$$

The time integral of the last equation gives the water surface elevation and the half width of the wetted area c. The impact pressure on the wedge is determined from Bernoulli's equation as:

$$\frac{p(x)}{\rho} = \frac{\partial\phi}{\partial t} - \frac{1}{2}(\nabla\phi)^2 = \sqrt{c^2-x^2}\,\frac{\mathrm{d}V}{\mathrm{d}t} + V\frac{c}{\sqrt{c^2-x^2}}\,\frac{\mathrm{d}c}{\mathrm{d}t} - \frac{1}{2}\,\frac{V^2x^2}{c^2-x^2} \tag{4.104}$$

Wagner's theory can be applied to arbitrarily shaped bodies as long as the deadrise angle is small, but not so small that air trapping plays a significant role. Wagner's theory is simple and useful, even if the linearization is sometimes criticized for its inconsistency as it retains a quadratic term in the pressure equation. This term is indispensable for the prediction of the peak impact pressure, but it introduces a singularity at the edge of the expanding plate ($x = \pm c$) giving negative infinite pressure there. Many experimental studies have checked the accuracy of Wagner's theory. Measured peak impact pressures are typically a little lower than estimated. This suggested that Wagner's theory gives conservative estimates for practical use. However, a correction is needed on the peak pressure measured by pressure gauges with finite gauge area. Special numerical FEM analyses of the local pressure in a pressure gauge can be used to correct measured data. The corrected peak pressures agree well with estimated values by Wagner's theory. Today, Wagner's theory is believed to give accurate peak impact pressure for practical use, albeit only for suitable hull forms with small deadrise angles.

The singularity of Wagner's theory can be removed taking spray into account. An 'inner' solution for the plate is asymptotically matched to an 'outer' solution of the spray region, as, for example, proposed by Watanabe in Japan in the mid-1980s (Fig. 4.20). The resulting equation for constant falling velocity is consistent and free from singularities. Despite this theoretical improvement, Watanabe's and Wagner's theories predict basically the same peak impact pressure (Fig. 4.21).

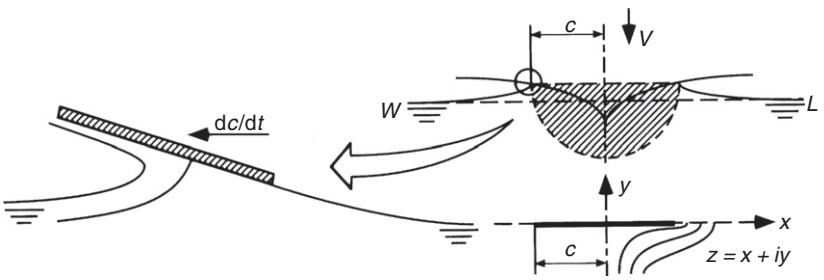

Figure 4.20:
Water impact model of Watanabe

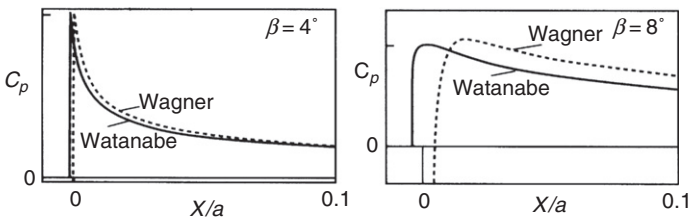

Figure 4.21:
Spatial impact pressure distribution

- *Simple non-linear slamming theories based on self-similar flow*
  We consider the flow near the vertex of a two-dimensional body immediately after water penetration. We can assume:
  - Near the vertex, the shape of the two-dimensional body can be approximated by a simple wedge.
  - Gravity accelerations are negligible compared to fluid accelerations due to the impact.
  - The velocity of the body V_0 is constant in the initial stage of the impact.

  Then the flow can be considered as self-similar depending only on x/V_0t and y/V_0t, where x, y are Cartesian coordinates and t is time. Russian scientists have converted the problem to a one-dimensional integral equation for $f(t)$. The resulting integral equation is so complicated that it cannot be solved analytically. However, numerically it has been solved by Faltinsen in Norway up to deadrise angles $\beta \geq 4°$. The peak impact pressure for $\beta = 4°$ was almost identical (0.31% difference) to the value given by Wagner's theory.
- *Slamming theories including air trapping*
  So far slamming theories have neglected the density of air, i.e. if a deformation of the free surface was considered at all it occurred only after the body penetrated the water surface. The reality is different. The body is preceded by an air cushion that displaces water already before the actual body entry. Air plays an even bigger role if air trapping occurs. This is especially the case for breaking wave impacts. In the 1930s, Bagnold performed pioneering work in the development of theories that consider this effect. Bagnold's impact model is simply constructed from added mass, a rigid wall, and a non-linear air cushion between them (Fig. 4.22). This model allows qualitative predictions of the relation between impact velocity V_0, air cushion thickness H, and peak impact pressure. For example, the peak impact pressure is proportional to V and $\sqrt{H}$ for slight impact and weak non-linearity of the air cushion; but for severe impact, the peak impact pressure is proportional to V^2 and H. These scaling laws were validated by subsequent experiments.

  Trapped air bottom slamming is another typical impact with air cushion effect. For two-dimensional bodies, air trapping occurs for deadrise angles $\beta \leq 3°$. Chuang's (1967) experiment for two-dimensional wedges gave peak impact pressures as in Table 4.3. The

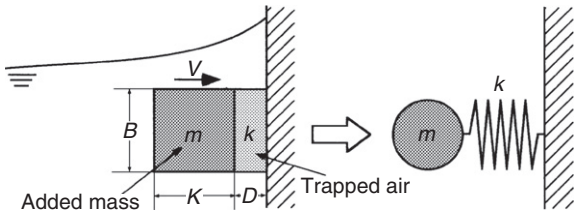

Figure 4.22:
Bagnold's model

Table 4.3: Chuang's (1967) relation for peak impact pressures

β	0°	1°	3°	6°	10°	15°	≥18°
P_{peak} (kPa)	$102V$	$115V^{1.4}$	$189V^{1.6}$	$64.5V^2$	$31V^2$	$17.8V^2$	Wagner's theory

impact velocity V is given in m/s. For $\beta = 0°$ air trapping is significant and the peak impact pressure is proportional to V. Increasing the deadrise angle reduces the amount of air trapping and thus the non-linearity. For practical use, the peak impact pressure is usually assumed to be proportional to V^2 for all β. This results in a conservative estimate.

Johnson and Verhagen developed two-dimensional theories for bottom impact with air trapping considering one-dimensional air flow between water surface and bottom to estimate the water surface distortion and the trapped air volume (Fig. 4.23).

The peak impact pressure thus estimated was much higher than measured. This disagreement results from the boundary condition at the edge of the flat bottom, where a jet emits to the open air. The theory assumes that the pressure at the edge is atmospheric pressure. This lets the air between water surface and bottom escape too easily, causing an underestimated trapped air volume. Experiments showed that the pressure is higher than atmospheric. Yamamoto has therefore proposed a modified model using a different boundary condition.

Experiments at the Japanese Ship Research Institute observed the trapped air impact with high-speed cameras and measured the initial thickness of air trapping. It was much thicker than the estimates of both Verhagen and Yamamoto. The reason is that a mixed area of air and water is formed by the high-speed air flow near the edge. Since the density of this mixed area is much higher than that of air, this area effectively chokes the air flow increasing air trapping.

The mechanism of wave impact with air trapping is in reality much more complicated. Viscosity of air, the effect of air leakage during compression, shock waves inside the air flow, and the complicated deformation of the free surface are all effects that may play an important role. Computational fluid dynamics may be the key to significant success here, but has not yet progressed sufficiently.

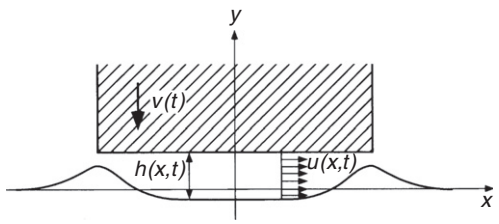

Figure 4.23:
One-dimensional air flow model of Verhagen

- *Effect of water compressibility*
  When a blunt body drops on calm water or a flat bottom drops on a smooth wave crest, usually no air trapping occurs. Nevertheless, one cannot simply use Wagner's theory, because at the top of such a blunt body or wave crest the relative angle between body and free surface becomes zero. Then both Wagner's and Watanabe's theories give infinite impact pressure. In reality, compressibility of liquid is important for a very short time at the initial stage of impact, when the expansion velocity of the wet surface dc/dt exceeds the speed of sound for water ($c_w \approx 1500$ m/s) producing a finite impact pressure. Korobkin (1996) developed two-dimensional theories which consider compressibility and free-surface deformation. For parabolic bodies dropping on the calm-water surface, he derived the impact pressure simply as $P = \rho c_w V$. Korobkin's theory is far more sophisticated, also yielding the time history of the pressure decay, but will not be treated here.
- *Three-dimensional slamming theories*
  All slamming theories treated so far were two-dimensional, i.e. they were limited to cross-sections (of infinite cylinders). Slamming for real ships is a strongly three-dimensional phenomenon due to, for example, pitch motion and cross-sections in the foreship changing rapidly in the longitudinal direction. Traditionally, approaches were used that obtain quasi three-dimensional solutions based on strip methods or high-speed strip methods. At the University of Michigan, Troesch developed a three-dimensional boundary element method for slamming. However, the method needs to simplify the physics of the process and the geometry of body and free surface and failed to show significant improvement over simpler strip-method approaches when compared to experiments.

  Limiting oneself to axisymmetric bodies dropping vertically into the water makes the problem de facto two-dimensional. The study of three-dimensional water impact started from the simple extension of Wagner's theory to such cases. The water impact of a cone with small deadrise angle can then be treated in analogy to Wagner's theory as an expanding circular disk. A straightforward extension of Wagner's theory by Chuang over-predicts the peak impact pressure. Subsequent refinements of the theory resulted in a better estimate of the peak impact pressure:

$$p(r) = \frac{1}{2}\rho V^2 \left(\frac{2}{\pi}\right)^2 \left[\frac{4\cot\beta}{\sqrt{1 - r^2/c^2}} - \frac{r^2/c^2}{1 - r^2/c^2}\right] \tag{4.105}$$

  r and c correspond to x and c in Fig. 4.19. This equation gives about 14% lower peak impact pressures than a straightforward extension of Wagner's theory. Experiments confirmed that the impact pressure on a cone is lower than that on a two-dimensional wedge of the same deadrise angle. So the three-dimensional effect reduces the impact pressure at least for convex bodies. This indicates that Wagner's theory gives conservative estimates for practical purposes. Since the impact on a ship hull is usually a very local phenomenon, Wagner's equation has also been used for three-dimensional surfaces using local relative velocity and angle between ship hull and water surface.

Watanabe (1986) extended his two-dimensional slamming theory to three-dimensional oblique impact of flat-bottomed ships. This theory was validated in experiments observing three-dimensional bottom slamming with a high-speed video camera and transparent models. Watanabe classified the slamming of flat-bottomed ships into three types:

1. Slamming due to inclined re-entry of the bottom. The impact pressure runs from stern to bow. No air trapping occurs.
2. Slamming due to vertical (orthogonal) re-entry of the bottom to a wave trough with large-scale air trapping.
3. Slamming due to vertical (orthogonal) re-entry of the bottom to a wave crest with only small-scale, local air trapping.

Type 1 (typical bottom impact observed for low ship speed) can be treated by Watanabe's three-dimensional theory. Type 3 (typical for short waves and high ship speed) corresponds to Chuang's theory for very small deadrise angle. Type 2 (also typical for short waves and high ship speed) corresponds to Bagnold's approach, but the air trapping and escaping mechanisms are different to simple two-dimensional models.

- *Hydro-elastic approaches in slamming*

It is important to evaluate not only peak impact pressures but also structural responses to the impact, to consider the impact pressure in the design of marine structures. Whipping (large-scale, weakly dampened oscillations of the longitudinal bending moment) is a typical elastic response to impact. In the late 1960s and 1970s, slamming and whipping resulted in some spectacular shipwrecks, e.g. bulkers and container ships breaking amidships. The disasters triggered several research initiatives, especially in Japan, which eventually contributed considerably to the development of experimental and numerical techniques for the investigation of slamming and whipping.

Let us denote the slamming impact load as $Z(t)$ and the elastic response of a ship as $S(t)$. Assuming a linear relation between them, we can write:

$$S(t) = \int_0^\infty h(t-\tau)Z(\tau)\,\mathrm{d}\tau \tag{4.106}$$

$h(\tau)$ is the impulse response function of the structure. An appropriate modeling of the structure is indispensable to compute $h(\tau)$. For example, the large-scale (whipping) response can be modeled by a simple beam, whereas small-scale (local) effects can be modeled as panel responses. For complicated structures, FEM analyses determine $h(\tau)$.

When the duration of the impact load is of the same order as the natural period of the structure, the hydro-elastic interaction is strong. The impact load on the flexible bottom can be about twice that on the rigid bottom. Various theories have been developed, some including the effect of air trapping, but these theories are not powerful enough to explain experimental data quantitatively. Coupling free-surface RANSE solvers and

FEM to analyze both fluid and structure simultaneously should improve considerably our capability to analyze hydro-elastic slamming problems within the next decade.

- *CFD for slamming*
  For most practical impact problems, the body shape is complex, the effect of gravity is considerable, or the body is elastic. In such cases, analytical solutions are very difficult or even impossible. This leaves CFD as a tool. Due to the required computer resources, CFD applications to slamming appeared only since the 1980s. While the results of boundary element methods for water entry problems agree well with analytical results, it is doubtful whether they are really suited to this problem. Real progress is only likely with field methods. Various researchers have approached slamming problems, usually employing surface-capturing methods. The three-dimensional treatment of slamming has benefited greatly from the rapid increase in computing power. State-of-the-art analyses by 2010 used three-dimensional, free-surface RANSE simulations for rigid-body motions. These capture impact forces well enough for whipping analyses (hull girder vibration triggered by slamming impacts). Local pressure peaks are still not captured well, as local hydro-elasticity is not considered.

4.6. Roll Motion

4.6.1. Linear, Undamped Free Roll

A heeled ship in smooth water will return to its original upright position due to the restoring (or righting) moment $m \cdot g \cdot h(\varphi)$. However, due to its kinetic energy, the ship will roll beyond the upright position to a heel angle on the other side and from there back, etc. In the absence of damping, this oscillatory motion would continue forever. For small roll angles, the roll motion of such an undamped free roll motion in calm water is characterized by:

$$(m_{44} + a_{44}) \cdot \ddot{\varphi} + m \cdot g \cdot GM \cdot \varphi = 0 \tag{4.107}$$

$m_{44} = \theta_{xx}$ is the mass moment of inertia for roll, a_{44} the added (hydrodynamic) mass moment of inertia, typically 10% of m_{44}. The natural roll frequency is thus:

$$\omega_n = \sqrt{\frac{m \cdot g \cdot GM}{m_{44} + a_{44}}} = \sqrt{\frac{g \cdot GM}{k'^2_{xx}}} \tag{4.108}$$

The formula is valid up to roll angles $\varphi < 5°$. $k'_{xx} = \sqrt{(m_{44} + a_{44})/m}$ is the radius of inertia (with respect to the roll axis). The corresponding natural roll period (= period between two maximum positive roll angles) is $T_n = 2\pi/\omega_n$. Section 3.6 gives empirical formulae to estimate T_n. The relation for T_n is used to determine GM experimentally. The seaway changes the average metacentric height GM. In addition, larger roll angles introduce non-linear effects,

changing the roll period considerably; e.g. the roll period tends towards infinity if the roll angle is close to angles where the righting lever is again zero.

For symmetric ships, within linear ship seakeeping theories, the roll motion is coupled only to yaw and sway motions. The roll axis (i.e. the axis where the sway and yaw motions disappear, leaving pure roll) is typically approximately halfway between waterline and center of gravity, with slightly higher values aft and lower values forward.

4.6.2. Capsizing in Waves

Few cases of capsizing are attributed directly to wave-excited roll motions, but capsizing has quite often been attributed to cargo shifts triggered by strong roll. While only numerical methods like non-linear strip methods can give detailed quantitative information, simplified considerations help in giving some quick estimates and general guidelines.

In regular waves from abeam, for wave length much longer than the ship width, the ship response is quasi-static. Within linear theory, the roll angle is given by:

$$|\varphi| = |\widehat{u}_4| = \frac{1}{\sqrt{\left(1 - \left[\frac{\omega_e}{\omega_n}\right]^2\right)^2 + \left(2D\frac{\omega_e}{\omega_n}\right)^2}} \cdot k \cdot h \quad \text{with} \quad 2D = \frac{n_{44}}{(m_{44} + a_{44}) \cdot \omega_n} \tag{4.109}$$

The response amplitude operator $|\varphi|/(kh)$ features a maximum for $D \leq \sqrt{2}/2$ (at resonance) (Fig. 4.24). For $D > 1$ (very small GM), the damping prevents any oscillation. GM can then no longer be measured in a roll experiment as a roll period. Model tests show that the roll damping n_{44} is nearly constant up to roll angles of 10° and then increases.

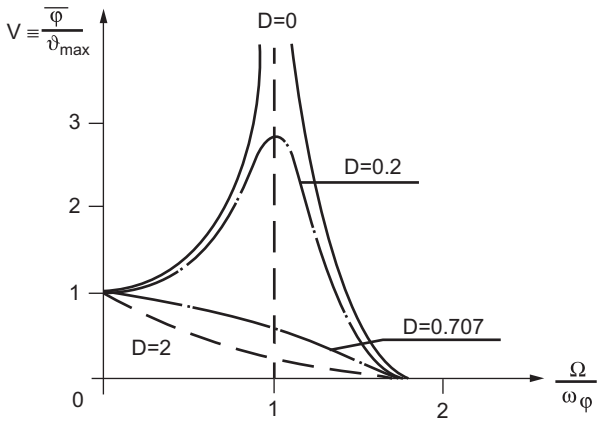

Figure 4.24:
Response amplitude operator for roll motion in waves from abeam

Non-linear effects often cannot be neglected in roll motion. For example, the restoring moment is only approximated by $m \cdot g \cdot GM$ for small angles, but for larger angles the real restoring moment curve has to be considered (Biran 2003). The solution of the resulting non-linear problem should be solved numerically. Different roll responses (roll angles) may then be obtained at a given exciting frequency, depending on whether the exciting frequency is approached from higher or from lower frequencies.

Following seas (and sometimes also head waves) may cause severe roll and even capsize for ships. In fact, following seas by themselves are more dangerous than beam seas. The resulting 'parametric excitation' can lead to severe rolling within a few roll periods, if the exciting frequency is near twice the natural roll frequency and metacentric heights vary greatly between hogging condition (ship in wave crest) and sagging condition (ship in wave trough). The righting lever in waves changes (for most ship hulls) with time, depending on the current waterline shape (Fig. 4.25). The slope of the curve at the origin is the metacentric height. Thus, for a ship in a seaway, there is no unique 'metacentric height' as for the ship in calm water. If people still use the word they implicitly mean the calm-water metacentric height.

Assuming a linear restoring moment, we write the fundamental differential equation for a free, undamped roll motion as:

$$(m_{44} + a_{44}) \cdot \ddot{\varphi} + m \cdot g \cdot GM \cdot \varphi = 0 \tag{4.110}$$

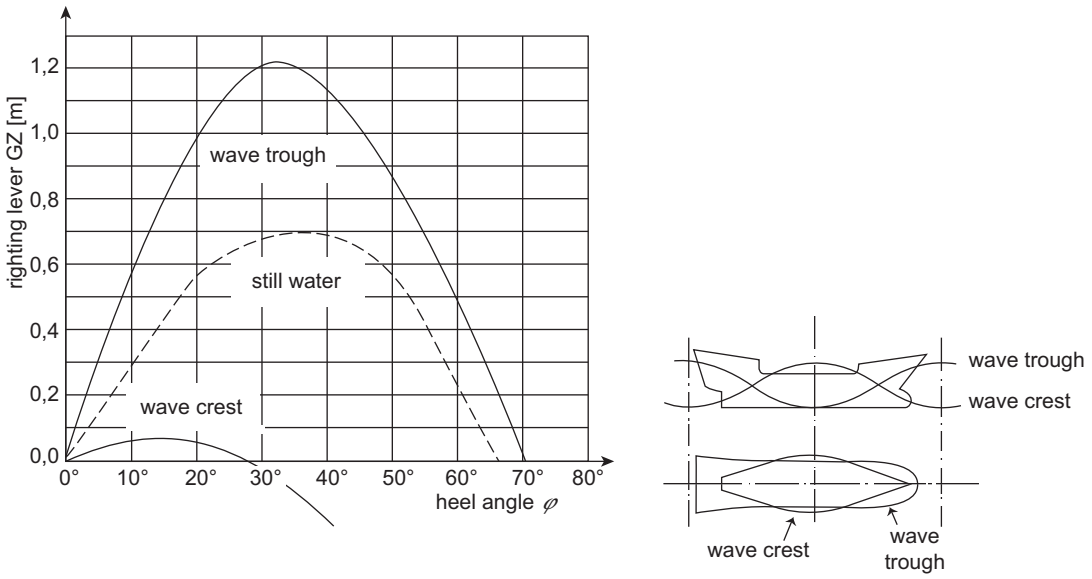

Figure 4.25:
Fluctuation of righting lever for ship in waves

The restoring moment now depends on a parameter, namely time t. The metacentric height is approximated to oscillate harmonically with exciting frequency ω_e:

$$GM(t) = GM_0 + \Delta GM \cdot \sin \omega_e t \tag{4.111}$$

This yields a so-called Mathieu equation:

$$\ddot{\varphi} + \omega_n^2 \cdot \left(1 + \frac{\Delta GM}{GM_0} \cdot \sin \omega_e t\right) \cdot \varphi = 0 \tag{4.112}$$

The solution of this differential equation features unstable areas where infinite amplitudes can be reached. For a ship, 'unstable response' means the ship capsizes. If ω_n/ω_e is close to a multiple of 1/2, the roll amplitudes can get infinitely large (resonance). The instability region increases as the fluctuation $\Delta GM/GM_0$ increases. Unstable areas can be plotted in a stability map (Strutt–Ince diagram, Fig. 4.26).

In reality, roll damping and non-linear restoring moments (righting moment curve) decrease the instability regions and roll amplitudes are no longer 'infinite'. With increasing frequency ratio, the amplitude decreases, making $\omega_n/\omega_e = 0.5$ (i.e. $\omega_e = 2\ \omega_n$) most critical.

The irregularity of real seaway makes parametric excitation less critical compared to regular waves in laboratory conditions, but still accidents due to parametric rolling have been reported at a rate showing that the phenomenon is not considered enough. A modern approach consists of selecting assorted time histories of representative seaways and using time-domain simulation tools to predict rolling of ships. Typically, rather than using long simulation times for 'normal' seaways, one then selects extreme seaways (e.g. with ten times the significant wave height for a given region) and simulates rather short times, comparing hull forms with respect to how often they capsize.

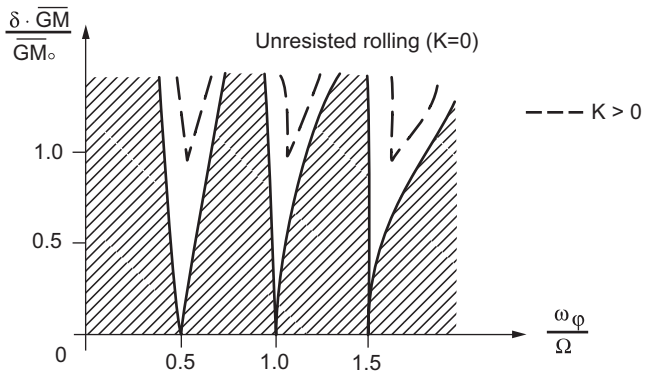

Figure 4.26:
Ince–Strutt diagram (stability map of Mathieu equation) plotting stable regions as shaded areas, linear restoring moment, without damping (solid lines) and with damping (dotted lines)

Parametric roll can be in practice a concrete danger if all the following conditions coincide:

1. The hull features large fluctuations of *GM* (between sagging and hogging conditions) (Fig. 4.4). Critical with respect to parametric roll excitation are hull forms with low block coefficient and large sectional flare at the ship ends like many modern hulls including container ships, ro-ro ferries, combatants, etc. The large change in waterline area between sagging and hogging then results in large changes of *GM*. The fluctuations are largest for wave lengths near ship length.
2. The ship speed *U* is such that the maximum of the encounter spectrum is near twice the natural roll frequency. For most ships, following and quartering seas are most critical. For large container ships, head waves can be critical. These ships are then excited to large pitch motions which increase the fluctuations of the metacentric height.

Large roll motions and accelerations, harmful to ship, cargo and humans (crew and passengers), may be avoided by:

(a) avoiding hull shapes with large difference in *GM* between ship in wave crest and ship in wave trough;
(b) shifting natural roll frequency to prevent resonance (changing *GM*);
(c) shifting exciting frequency (changing course or speed);
(d) increasing damping by active systems (foils, tanks).

Advance warning systems combining information on sea state and ship data with some simple rules are commercially available.

4.6.3. Roll Damping

Roll damping is usually weak. As a consequence, response amplitude operators for roll have a pronounced maximum near natural roll frequency. This is different for pitch and heave response amplitude operators which feature typically only weak and sometimes no local maxima. All computational methods, even simple strip methods, consider wave radiation and the associated damping. However, wave radiation is only for multi-hulls, an effective damping mechanism. For rotational bodies rolling around their axis of rotation, the wave radiation and associated damping is zero. For usual ship geometries, it is negligibly small.

The shear stress (tangential friction) on the hull is also negligible at zero speed. At forward speed, the damping moment can be estimated as:

$$M_{\mathrm{roll},f} = R_f \frac{\omega_r u_4}{V} R^2 \tag{4.113}$$

R_f is the frictional resistance of the ship following ITTC'57, ω_r the actual roll frequency, V the ship speed, u_4 the roll amplitude, and R is the average distance of the hull surface to the roll axis.

The roll motion induces an oblique flow at the rudder (at center position). This in turn creates a rudder force which dampens the roll motion. The angle of attack is approximately

$$\alpha = \frac{\omega_r \cdot z}{V} \cdot u_4 \tag{4.114}$$

where z is the distance of a point on the rudder from the roll axis. We assume that the effects of wake (reducing the inflow speed) and propeller slipstream (increasing the inflow speed) cancel each other approximately. In addition, we neglect the oblique flow induced by the rolling ship and the propeller in oblique flow. We employ the usual estimate for the lift coefficient at the rudder (in rough approximation as this formula is valid for uniform flow with constant angle of attack over the height). Then we get for the roll damping moment due to the rudder:

$$M_{\text{roll,rudder}} = \omega_r \cdot u_4 \cdot \frac{\Lambda(\Lambda + 0.7)}{(\Lambda + 1.7)^2} \cdot \pi \cdot \rho \cdot V \cdot I_R \tag{4.115}$$

I_R is the areal moment of inertia of the rudder area with respect to the roll axis.

For a rectangular rudder, $I_R = c(z_2^3 - z_1^3)/3$; c is the chord length of the rudder. z_1 indicates the upper edge of the rudder, z_2 its lower edge. Λ is the rudder aspect ratio, c the chord length. Controlled rudder action can be used to actively dampen roll motions. Some course interference and added resistance must then be accepted. Similarly, Voith−Schneider propellers can be used to dampen roll motions. Unlike rudders, the VSP is also effective at zero forward speed.

Similar to the rudder, an immersed transom stern creates a roll damping moment for the ship at forward speed. We can use an equivalent formula as for the rudder, but employ the immersed beam instead of the rudder height. However, as the hull has water only on the underside, a factor 0.5 has to be applied:

$$M_{\text{roll,transom}} = \frac{1}{2} \omega_r \cdot u_4 \cdot \frac{\Lambda_t(\Lambda_t + 0.7)}{(\Lambda_t + 1.7)^2} \cdot \pi \cdot \rho \cdot V \cdot I_{R,t} \tag{4.116}$$

$\Lambda_t = B_t/(2L_{pp})$ (where B_t is the transom beam in the waterline) and $I_{R,t} = B_t^3 L_{pp}/12$.

Because the damping mechanisms discussed so far are rather weak (particularly at low speed), ships typically employ additional means to increase roll damping. These are discussed in the following.

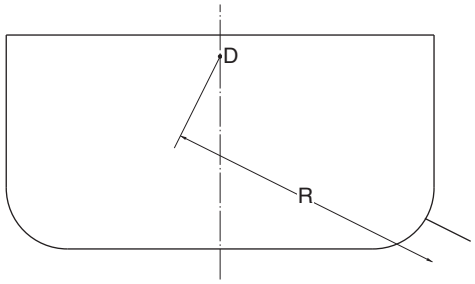

Figure 4.27:
Definition of *R*. *D* indicates the roll axis

Bilge keels are fitted on most ships. Bilge keels are narrow strips extending along the central part of the ship in the bilge region. They project no further than the width and depth of the ship to prevent contact damage. The effect of the bilge keels depends hardly on the ship speed. The damping moment can be estimated following:

$$M_{\text{roll,bilge}} = 2 \cdot \frac{\rho}{2} \cdot w^2 \cdot C_D \cdot l_{bk} \cdot h_{bk} \cdot R \tag{4.117}$$

l_{bk} is the length of the bilge keel, h_{bk} its height, C_D a resistance coefficient. Figure 4.27 shows the definition of R. The factor 2 considers that we have bilge keels on port and on starboard. w is the transverse relative flow speed found approximately at half keel height if there were no bilge keel:

$$w \approx \omega_r \cdot u_4 \cdot R \cdot k \tag{4.118}$$

The factor k considers the local flow changes in the bilge region (Fig. 4.28). Bilge keels are not very effective in comparison to even the passive roll damping of the rudder at design speed, but are still necessary for zero or low speed. Bilge keels also increase exciting forces (and resistance). For ships with effective alternative damping mechanisms (fins, tanks), one should then rather omit bilge keels. If the roll motion is largely suppressed, only the negative effect of increased exciting forces remains. The only argument left is then having a back-up in case of failure of the other more complex systems.

Blume (1979) gives the following values for C_D, depending on the amplitude of relative motion between bilge keel and water, $x_0 \approx u_4 \cdot R \cdot k$:

x_0/h_{bk}	0.4	0.8	1.2	1.6	2	3	4	6	8
C_D	11.7	9.6	7.8	7.0	6.5	5.0	4.3	3.6	3.2

Fin stabilizers are usually arranged symmetrically near the bilge, approximately amidships. The fins are tilted around an axis perpendicular to the ship to create a roll damping moment.

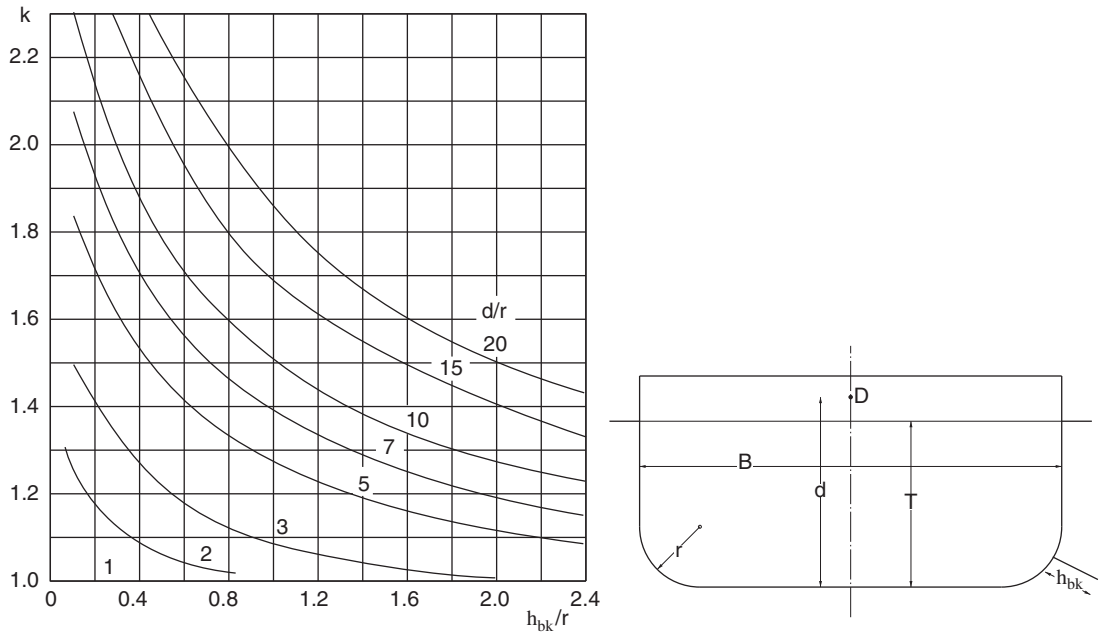

Figure 4.28:
Factor k for local flow speed in bilge region with dimensions as appearing in the diagram

The fins are usually retractable (to avoid damage in port). The damping moment furnished by a pair of fins can be estimated as

$$M_{\text{roll,fin}} = 2 \cdot \frac{\rho}{2} \cdot V^2 \cdot C_L \cdot A_{\text{fin}} \cdot R \tag{4.119}$$

R is the leverage as shown in Fig. 4.27, A_{fin} the fin area. The lift coefficient as function of angle of attack α can be estimated by:

$$C_L = 1.6 \left(2\pi \frac{\Lambda_{\text{eff}} \cdot (\Lambda_{\text{eff}} + 0.7)}{(\Lambda_{\text{eff}} + 1.7)^2} \cdot \sin \alpha + \sin \alpha \cdot |\sin \alpha| \cdot \cos \alpha \right) \tag{4.120}$$

Λ_{eff} is the effective side ratio of the fin. If there is (almost) no flow around the edge of the fin at the hull (due to small gap), we have $\Lambda_{\text{eff}} \approx 2\Lambda$. The factor 1.6 considers that stabilizing fins are usually flapped rudders where the aft flap turns by approximately 2δ if the main forward foil turns by δ. For single-foil fins the factor is 1. The maximum lift coefficient $C_{L,\max}$ lies typically between 3 and 3.5, provided that sufficiently high angles of attack are obtained.

The fin angle δ differs from the angle of attack α. Considering just the roll motion of the ship and assuming δ in phase with the roll velocity, we have:

$$\alpha = \delta + \arctan \frac{\omega_r \cdot u_4 \cdot R \cdot k}{V} \tag{4.121}$$

The fins are rather ineffective at low speed. At high speeds, a theoretical maximum $C_{L,\max}$ cannot be obtained due to structural overloading of the shaft and its supports. Therefore δ has to be limited to smaller values at higher speeds.

Roll stabilizing tanks are cheaper than fins and also effective at low speeds. This comes at the expense of larger weight (including the necessary water in the tanks), larger volume and a reduction of the metacentric height due to the free-surface effects. Unless special measures are taken, roll stabilizing tanks can also cause noise, which is particularly disturbing if the ship is transporting passengers. There are in principle two types of tanks: U-shaped tanks consist of two narrow tanks located at port and starboard, connected via the double bottom. Flume tanks are tanks with a free surface over the complete ship's width. In either case the tanks are partially filled, allowing the water to slosh from one side to the other. If the lowest natural frequency of the water sloshing coincides with the roll natural frequency of the ship and the ship is excited at this frequency by the waves the ship is excited to roll motion with a phase shift of 90° to the exciting waves and the sloshing water with another phase shift of 90° to the roll motion, yielding a total phase shift of 180° between exciting wave moment and damping tank moment. Ideally, the ship rests almost calm and the seaway excites only an oscillation of the water in the tank.

U-shaped tanks create a roll damping moment:

$$M_{\text{roll,tank}} = \rho \cdot g \cdot A_0 \cdot h_{\text{col}} \cdot B_1 \tag{4.122}$$

A_0 is the horizontal cross-section area of one side of the symmetric tank. The water level rises and falls by $\pm h_{\text{col}}$, without touching the top or the connecting pipe at the bottom. $B_1 < B$ is the horizontal distance of the tank centers on both sides. The natural frequency of such a tank can be estimated within the framework of a simple flow tube theory:

$$\omega_{n,\text{tank}} = \sqrt{\frac{2g}{A_0 \int_0^S \frac{1}{A}\,\mathrm{d}s}} \tag{4.123}$$

$A(s)$ is the local cross-section area at the local one-dimensional flow coordinate s, S the total length of the flow tube. The formula shows that the dimensions of the connecting pipe influence the natural frequency. Once installed, different filling heights allow only small changes in natural frequency and come at the possible expense of reducing the maximum sloshing height h. A better strategy is therefore to design the tank such that the natural frequency is above the highest natural roll frequency and then retard the tank water motion in operation. The retard can be realized either by direct valves in the connecting pipe or (better) by controlling the air in the tanks above the water.

Flume tanks are typically rectangular tanks which extend over the whole ship width and are partially filled. They require more space and weight than U-shaped tanks, but can dampen wider ranges of frequencies without active control due to the effective damping in wave breaking. The natural frequency of a flume tank is approximately (for small water depth H compared to tank width b):

$$\omega_n = \frac{\pi\sqrt{gH}}{b} \tag{4.124}$$